

CHRISTIAN MICHAEL SCHRADER
Geochronology and Geology of the Pebble Cu-Au-Mo Porphyry and the Sill Au-Ag
Epithermal Deposits, Southwest Alaska
(Under the Direction of DOUGLAS E. CROWE)

The Late Cretaceous Pebble Cu-Au-Mo deposit is a large Cu and Au resource within a belt of Cu and Au deposits in southwest Alaska. This study presents precise $^{40}\text{Ar}/^{39}\text{Ar}$ igneous and alteration ages and a Re-Os mineralization age from the Pebble deposit as well as an alteration age from the Tertiary Sill epithermal Au-Ag deposit, which is less than 5 km from the Pebble deposit. These data have utility in regional exploration modeling and provide an opportunity to relate the timing of intrusion to alteration and mineralization.

The geologic and geochronologic data document Cretaceous igneous and hydrothermal events from ~96 Ma to 83.5 Ma. These include 1) an early suite of biotite-magnetite-pyroxenites and diorite dated at 95.9 ± 0.3 to 95.3 ± 0.3 Ma, 2) a molybdenum mineralization event in the porphyry stocks dated at 89.5 ± 0.3 Ma, 3) potassic alteration related to copper mineralization dated at 88.5 ± 0.3 Ma (biotite) and 86.0 ± 0.3 Ma (K-feldspar), and 4) a hypabyssal syenite intrusion dated at 84.1 ± 0.3 Ma. The range of mineralization and alteration ages is due in part to the lower closure temperatures of the alteration silicate minerals relative to molybdenite, and in part to protracted hydrothermal circulation from multiple porphyry stocks. Over 35 m.y. later, in the Tertiary, the Sill latite host rock crystallized and the Sill epithermal mineralizing event occurred.

INDEX WORDS: Pebble Cu-Au Deposit, Alaska, Iliamna, Porphyry copper, Geochronology, $^{40}\text{Ar}/^{39}\text{Ar}$, Re-Os, Alkaline igneous rocks.

GEOCHRONOLOGY AND GEOLOGY OF THE PEBBLE CU-AU-MO PORPHYRY
AND THE SILL AU-AG EPITHERMAL DEPOSITS, SOUTHWEST ALASKA

by

Christian Michael Schrader

B.S., The University of Georgia, 1998

A Thesis Submitted to the Graduate Faculty of The University of Georgia in Partial
Fulfillment of the Requirements for the Degree

MASTERS OF SCIENCE

ATHENS, GEORGIA

2001

© 2001

Christian Michael Schrader

All Rights Reserved

GEOCHRONOLOGY AND GEOLOGY OF THE PEBBLE CU-AU-MO PORPHYRY
AND THE SILL AU-AG EPITHERMAL DEPOSITS, SOUTHWEST ALASKA

by

Christian Schrader

Approved:

Major Professor: Douglas E. Crowe

Committee: Mike Roden

Sam Swanson

Electronic Version Approved:

Gordhan L. Patel

Dean of the Graduate School

The University of Georgia

December 2001

ACKNOWLEDGEMENTS

This research was funded by Cominco American, Inc. and grants from the Society of Economic Geology and The University of Georgia's Wheeler-Watts fund.

Thank you to my advisor, Doug Crowe, for his patience and help. Thanks to the members of my committee, Mike Roden and Sam Swanson, for their reviews and helpful criticisms. Thanks to Jim Whitney for his insight during the early months of my work.

Thank you to Paul Layer and Jeff Drake for teaching me almost everything I know about $^{40}\text{Ar}/^{39}\text{Ar}$ dating while I was an undergraduate, and for their support and expertise throughout this project. Thank you to Holly Stein for running my Re-Os analysis and for her help with interpreting my data. Thanks to Rainer Newberry for being such an important and supportive influence during my undergraduate career. And most of all, thank you to my friends and family for supporting me during this process.

TABLE OF CONTENTS

	Page
ACKNOWLEDGEMENTS.....	6
LIST OF TABLES.....	vii
LIST OF FIGURES	viii
SECTION	
1. INTRODUCTION	1
2. REGIONAL GEOLOGY	5
3. DEPOSIT GEOLOGY	8
Pre-ore igneous rocks.....	8
Igneous rocks contemporaneous with ore.....	23
The porphyry suite, hydrothermal alteration and mineralization.....	19
Post-ore rocks.....	26
4. METHODS	29
Plateau and Pseudo-plateau Definitions.....	30
5. GEOCHRONOLOGY SAMPLE DESCRIPTIONS	33
6. RESULTS	36
Geochronology.....	36
Geochemistry	45
7. DISCUSSION	51
Geochronology.....	51
Geochemistry	54
8. CONCLUSIONS.....	71
REFERENCES	77

APPENDICES

A. Electron microprobe analyses	77
B. Data tables for $^{40}\text{Ar}/^{39}\text{Ar}$ step heating analyses.....	85
C. Summary drill hole logs of selected holes	93

LIST OF TABLES

TABLE.....	Page
1. Summary of $^{40}\text{Ar}/^{39}\text{Ar}$ and Re-Os geochronology.....	14
2. Re-Os age for molybdenite from the Pebble Cu-Au porphyry deposit	37
3. Whole rock geochemical data and CIPW norms for Pebble lithologies.....	46
4. Whole rock and trace element geochemical data and CIPW norms for selected Pebble samples.....	49

LIST OF FIGURES

FIGURE	Page
1. Map of southcentral Alaska	2
2. Lithotectonic terranes of southern Alaska	6
3. Geologic map of the Pebble deposit and the surrounding area.....	9
4. Detailed map of Pebble deposit	12
5. Photomicrographs Kbp and Ksy lithologies (Figure 5a-h).....	16
6. Backscatter electron microprobe image from Sill sample S-122.....	27
7. Figures 7a-7g of $^{40}\text{Ar}/^{39}\text{Ar}$ age spectra	38
8. Plot of $\text{Al}_2\text{O}_3/\text{TiO}_2$ vs. SiO_2 for lithologies found within the Pebble deposit.	55
9. Plot of $\text{Al}_2\text{O}_3/\text{TiO}_2$ vs. TiO_2 for lithologies found within the Pebble deposit..	57
10 $\text{Na}_2\text{O}+\text{K}_2\text{O}$ vs. SiO_2 diagram for post-mineralization Ksy sample	60
11. Harker diagrams for the post-Ksy samples.....	62
12. Fenner diagram for the Kbp series and sample PB-108	65
13. Chondrite-normalized rare earth element (REE) spider diagrams	68

SECTION 1

INTRODUCTION

The Pebble Cu-Au-Mo and the Sill epithermal Au-Ag deposits are located within the largest single claim block in Alaska (Turner, personal communication, 1998). The Pebble deposit, roughly in the center of the block, is at 59°53'54'' N latitude and 155°17'44'' W longitude in southwest Alaska, approximately 350 kilometers southwest of Anchorage and 30 kilometers northwest of the town of Iliamna. (Figure 1). The elevation of the deposit is 300-450 meters above sea level.

Cominco American, Inc. discovered the Pebble and Sill deposits in 1987 during a reconnaissance exploration program for epithermal and intrusive-hosted gold deposits. Pebble and Sill lie on a northeasterly trend 100 kilometers southwest of the dacite-related Kijik Cu-Ag-Mo deposit (Young et al., 1997), 160 kilometers southwest of the Rainy Pass shoshonitic Cu-Au deposit (Bouley et al., 1995) and 190 kilometers southwest of the granodiorite and diorite-related Neacola Cu-Mo deposit (Young et al., 1997).

Pebble contains a measured resource of 1 billion tonnes with grades of 0.30% Cu, 0.34 g/t Au and 200-300 ppm Mo, with a higher grade core of 54 million tonnes at 0.54% Cu and 0.46 g/t Au (annual reports – Cominco, 1997-1999). Sill, although high grade, proved early in the exploration process to be small, and Cominco concentrated their efforts on delineating the resource at Pebble. Porphyry-style alteration to the south of Pebble indicates the possible presence of additional mineralized stocks and the claim block has multiple Au and Cu soil anomalies that have not been fully defined (Bouley et al., 1995, Turner, oral communication, 1998). The known presence of porphyry and epithermal mineralization, the metal anomalies in the soil and the extensive alteration make the Pebble claim block an attractive target for further exploration.

Figure 1: Map of south central Alaska showing the location of Pebble and the town of Iliamna. Red box on inset map shows location of map within Alaska. Pebble is located approximately 325 km southwest of Anchorage. From Tracy (2001).



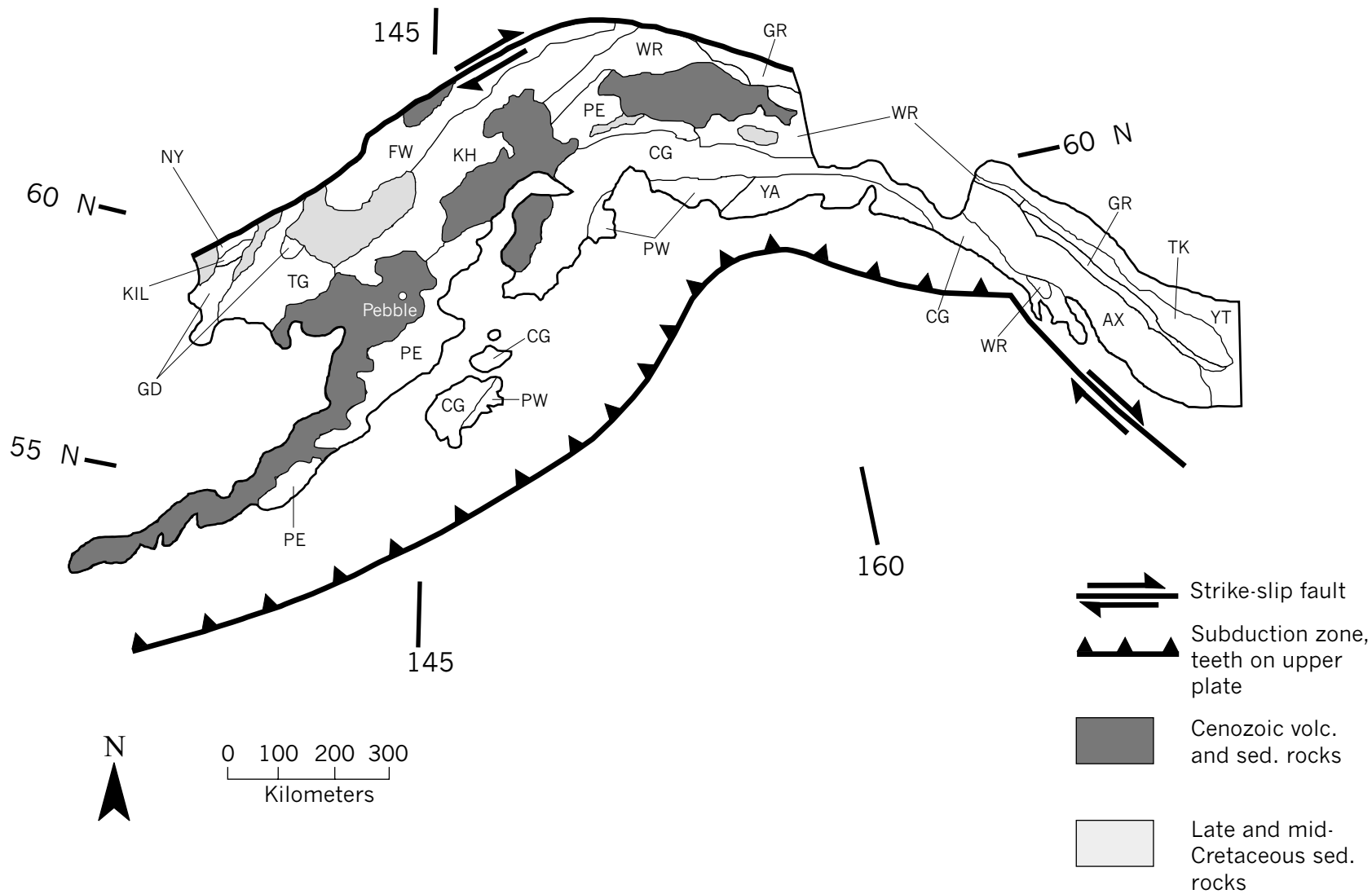
Surface exposures at Pebble and Sill are poor and confined mostly to weathered rubble outcrops, making geologic mapping and the definition of cross-cutting igneous relationships difficult. Even the extensive drilling at Pebble (~125 diamond drill holes) has failed to provide enough information to resolve many age relationships. The purpose of this study is to augment the existing exploration model with precise geochronology of alteration, mineralization and igneous crystallization of pre- and post-mineralization igneous rocks.

SECTION 2

REGIONAL GEOLOGY

The Pebble deposit claim block lies in the southern Kahlitna terrane (see Figure 2), to the west, inboard and near the border of the Peninsular terrane. The topography is dominated by the Alaskan-Aleutian Range batholith, which forms the mountainous spine of the Alaska peninsula. The Peninsular terrane is comprised of Permian to Triassic limestones, tuffs, cherts and clastic rocks, early to middle Jurassic intrusions, and middle Jurassic to Cretaceous sedimentary rocks. Cretaceous to Tertiary plutons and dikes intrude the Peninsular terrane near Pebble; these were followed by Tertiary to recent volcanic rocks, all of which are the product of continuous northwestward subduction along ancient trenches and the modern Aleutian trench (Bouley et al., 1995). The Kahlitna terrane is dominated by basinal turbidites thought to have been deposited from the west from the late Jurassic to the early Cretaceous, which overlie late Triassic basalts and andesites and are intruded by Cretaceous to Tertiary plutons (Detterman and Reed, 1980), including the intrusions that host the Pebble and Sill deposits. Since the Tertiary there has been sporadic volcanism, including basalt and andesite flows with lesser latite and andesitic to rhyolitic tuffs (Detterman and Reed, 1980). The compressional stress of the continuing northwest dipping subduction has resulted in northeast trending reverse and strike-slip faults, which define the structural grain of the Kahlitna and Peninsular terranes (Bouley et al., 1995.)

Figure 2: Lithotectonic terranes of southern Alaska, bounded on the north by the Denali-Farewell fault system, adapted from Goldfarb (1997). Sedimentary and volcanic rocks are shown where they cover and obscure lithotectonic boundaries. Terranes are: AX = Alexander, CG = Chugach, FW = Farewell, GD = Goodnews, GR = Gravina, KH = Kahiltna, KIL = Kilbuck, NY = Nyack, PE = Peninsular, PW = Prince William, TG = Togiak, TK = Taku, WR = Wrangellia, YA = Yakutat, and YT = Yukon-Tanana.



SECTION 3

DEPOSIT GEOLOGY

Figure 3 is a map of the geology around the Pebble and Sill deposits. Figure 4 is a map of the immediate area around the Pebble deposit. The following descriptions are taken largely from the overview by Bouley et al. (1995), and unpublished Cominco maps (Cominco annual report, 1994). Geologic mapping in the area is difficult due to the very limited outcrop exposure, and most mapping is based on rubble outcrops and collar lithologies in drill holes. The country rock in the area is part of the early Jurassic to middle Cretaceous sequence of siltstone, argillite and greywacke found throughout the southern Kahiltna terrane, which have been isoclinally folded and regionally metamorphosed to lower greenschist facies. Mafic volcanoclastic rocks are interlayered with the sediments. Much of the region is covered by quaternary gravels (Qg on Figure 3). The chronology discussed in this section is based on previous age dating, cross-cutting and stratigraphic relationships from Bouley et al. (1995) and unpublished Cominco reports; geochronology completed for this study is discussed in later sections.

Pre-ore igneous rocks

The pre-mineralization plutonic rocks in the area include small diorite bodies and a biotite magnetite pyroxenite body 4-5 km south of Pebble. The diorites (Kd) are found flanking Pebble to the northwest, and in drill core (no surface outcrop) flanking the biotite-magnetite pyroxenite to the northwest (see appendix 3 for relevant drill hole summaries). It is composed of hornblende and plagioclase with accessory magnetite and apatite. Texturally, it is dominantly porphyritic with phenocrysts of hornblende and plagioclase, but it is locally equigranular. Some samples of the diorite are propylitically altered (secondary calcite + epidote \pm pyrite), and

Figure 3: Geologic map of the Pebble deposit and the surrounding area, from rare outcrop, rubble outcrop and drill hole collar lithologies. This map is based on Cominco geologists' mapping (Cominco annual report, 1994), with minor adaptations by the author. The box in the upper middle defines the border of the deposit area and the region of most geologic mapping (shown in more detail in **Figure 4**). Contacts that are shown truncating against this border are artifacts of the spatial concentration of geologic mapping, i.e., contacts were not always followed beyond the deposit area. Small circular units just south of the deposit border are generated from drill hole collar intercepts. The Sill deposit lies at the southern end of the latite body.

This figure also contains text boxes with summaries of geochronologic data. Numbers in parentheses refer to **Table 1**. The numbers (9) and (10) refer to U-Pb ages previously obtained by Cominco American, Inc.

Legend

 Epithermal Au-qtz vein

 0.2% Cu contour

 Fault

 Qg gravel cover

 Kgde equigranular granodiorite

 Ts sandstone and conglomerate

 Kgdp porphyritic granodiorite

 Ta intermediate volcanic rocks

 Kqmp porphyritic and equigranular quartz monzonite and tonalite

 Tb mafic volcanic rocks

 Kd diorite

 Tl Sill Mountain latite

 Kdp porphyritic diorite

 TKf felsic tuff; exact age unknown

 Kbd biotite diorite

 Ksy syenite

 Kgb gabbro

 Kmp monzodiorite porphyry

 Kbp biotite-magnetite pyroxenite

 Kibx intrusive breccia

 Kh hornfelsed sediments

 Kqsp qtz-ser-py altered unit

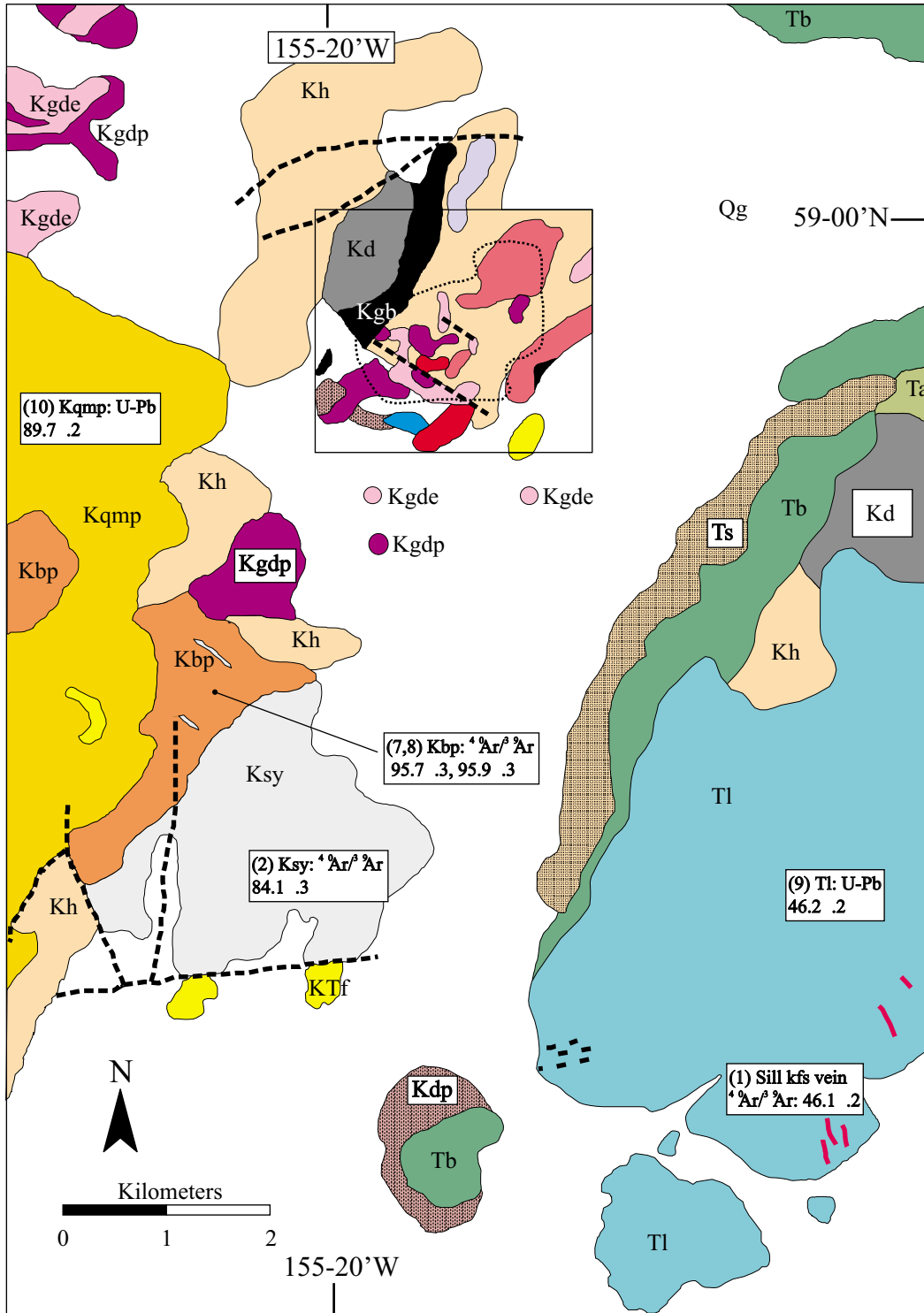
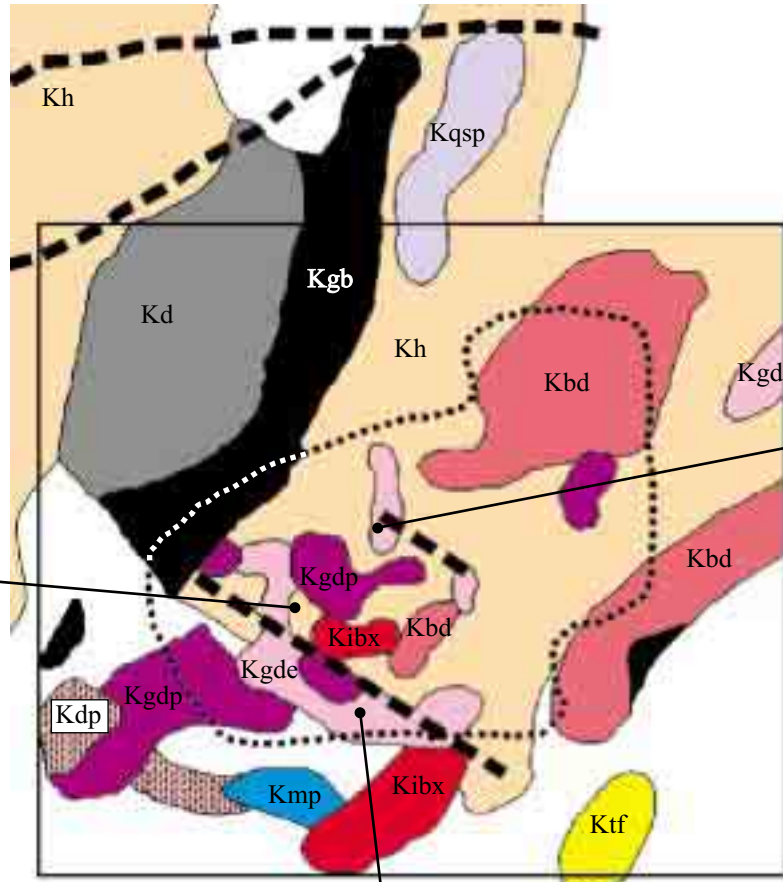


Figure 4: Detailed map of Pebble deposit, from the upper center of **Figure 3**, with an outline of the 0.2% Cu resource. Refer to the legend in **Figure 3**. Text boxes with summaries of geochronologic data, and point to the location of diamond drill hole locations (note that the collar lithologies mapped may not match sample lithology from depth.. Numbers in parentheses refer to **Table 1**.

vein kfs in Kbd:
 $^{40}\text{Ar}/^{39}\text{Ar}$
86.0 0.2 Ma

vein mb in Kqmp:
Re-Os
89.5 0.3 Ma

vein bt in Kibx:
 $^{40}\text{Ar}/^{39}\text{Ar}$
88.5 0.3 Ma



Kgde

Kgde



Kgd

0 0.5 1

Kilometers

Table 1: Summary of $^{40}\text{Ar}/^{39}\text{Ar}$ and Re-Os geochronology results. Shaded ages are those interpreted as most accurate. See Figure 7 for $^{40}\text{Ar}/^{39}\text{Ar}$ spectra. See text for description of “pseudo-plateau”.

Sample, host lithology	location	mineral dated	age
BMP-7 (8) (Kbp)	surface, “duck zone”, south of Pebble Main Zone	igneous biotite from biotite-magnetite pyroxenite, $^{40}\text{Ar}/^{39}\text{Ar}$	95.9 ± 0.3 Ma plateau 95.6 ± 0.6 Ma plateau isochron 96.2 ± 0.3 Ma integrated $^{40}\text{Ar}/^{36}\text{Ar}_i$: 314.0 ± 41.1
RK-3 (7) (Kbp)	surface, “duck zone”, south of Pebble Main Zone	igneous biotite from biotite-magnetite pyroxenite, $^{40}\text{Ar}/^{39}\text{Ar}$	95.7 ± 0.3 Ma plateau 96.0 ± 0.7 Ma plateau isochron 95.5 ± 0.3 Ma integrated $^{40}\text{Ar}/^{36}\text{Ar}_i$: 270.5 ± 44.7
PB-108 (6) (Kd)	DDH PB24, 144’	igneous hornblende from diorite, $^{40}\text{Ar}/^{39}\text{Ar}$	95.3 ± 0.3 Ma plateau 95.3 ± 0.5 Ma plateau isochron 95.2 ± 0.3 Ma integrated $^{40}\text{Ar}/^{36}\text{Ar}_i$: 293.4 ± 21.6
PB-83 (5) (Kgdp)	DDH PB39, 169’ Main Pebble Zone	molybdenite from qtz-moly-ser vein in Kgdp, Re-Os	89.5 ± 0.3 Ma
BJT-68 (4) (Kibx)	DDH PB28, 203’ Main Pebble Zone	alteration biotite from halo of cpy-bearing vein in igneous breccia $^{40}\text{Ar}/^{39}\text{Ar}$	88.5 ± 0.3 Ma plateau 88.6 ± 0.6 Ma plateau isochron 88.9 ± 0.3 Ma integrated $^{40}\text{Ar}/^{36}\text{Ar}_i$: 291.6 ± 54.1
PB-162 (3) (Kbd)	DDH PB78, 193’ Main Pebble Zone	kfs from cpy-bearing vein in biotite diorite, $^{40}\text{Ar}/^{39}\text{Ar}$	86.0 ± 0.2 Ma pseudo-plateau 86.1 ± 0.2 Ma pseudo-plateau isochron 86.1 ± 0.2 Ma integrated $^{40}\text{Ar}/^{36}\text{Ar}_i$: 303.4 ± 8.9
PB-79 (2) (Ksy)	DDH PB105, 74’ South zone	igneous biotite from syenite, $^{40}\text{Ar}/^{39}\text{Ar}$	84.1 ± 0.3 Ma pseudo-plateau 83.6 ± 0.7 Ma pseudo-plateau isochron 84.1 ± 0.3 Ma integrated $^{40}\text{Ar}/^{36}\text{Ar}_i$: 306.5 ± 9.0
S-91 (1) (TI)	DDH S19, 449’ Sill epithermal deposit	vein kfs in latite, $^{40}\text{Ar}/^{39}\text{Ar}$	46.6 ± 0.1 Ma pseudo-plateau 46.1 ± 0.2 Ma whole isochron 46.8 ± 0.2 Ma integrated $^{40}\text{Ar}/^{36}\text{Ar}_i$: 302.7 ± 1.5

it is possible that the biotite diorite described below in the section on the porphyry suite is a highly altered phase of this diorite.

The biotite magnetite pyroxenite (Kbp) unit is texturally and mineralogically variable. Photomicrographs of several phases of this rock are shown in Figure 5a-f. Every sample examined in this study contains diopside, magnetite and apatite. All but one sample contains primary biotite, or specifically phlogopite (Phl₆₅₋₇₇, see appendix 1), often as much as 20% by volume. Several of the samples from the surface (including those dated for this study) and drill core contain plagioclase as well. Though the pyroxenite phase is dominant, some phases contain enough plagioclase to be classified as plagioclase-bearing pyroxenites and, rarely, biotite-gabbros by the IUGS plutonic nomenclature for ultramafic rocks. The unit is not differentiated on the geologic map, and Cominco's Kbp label is used throughout this study. Additionally, some samples contain traces (<1 modal %) of orthopyroxene. This unit often shows weak to strong alignment of pyroxene, with less pronounced alignment of plagioclase and biotite. Several of the Kbp samples show variable cumulate relationships: always with early cumulate apatite, cumulate diopside and intercumulate magnetite. The temporal order of other minerals, when present, is less regular and in some cases there are multiple generations of magnetite and apatite. Several samples contain xenoliths of clinopyroxene-magnetite-apatite±biotite; mineral compositions of xenolith phases are typically similar to nearly identical to phases present in the host rock. Electron microprobe imaging and EDS analysis of one sample revealed 1-10 μm blebs and globules of primary (i.e., not associated with any later alteration) Cu-Fe and Cu-Ni-Fe sulfides. Although further investigation is beyond the scope of this study, these sulfides are intriguing, especially in light of work on primary sulfides in pre- and syn-ore rocks at Bingham and their possible role in ore formation (Keith et al., 1997) and work on Au-Cu mineralization associated with potassic rocks (Müller and Groves, 1995).

Figures 5A-H: Photomicrographs of samples from the biotite-magnetite pyroxenite (Kbp) lithology (**A-F**) and a syenite (Ksy) sample (**G-H**). Samples are in pairs in plane polarized light (PPL) on the top and crossed polarized light (XPL) on the bottom. For all samples, labels are as follows: Pl = plagioclase, Px = clinopyroxene, Bt = biotite, Mt = magnetite, Ap = apatite.

Figure 5A and 5B: Biotite-syeno-gabbro sample BMP-3.

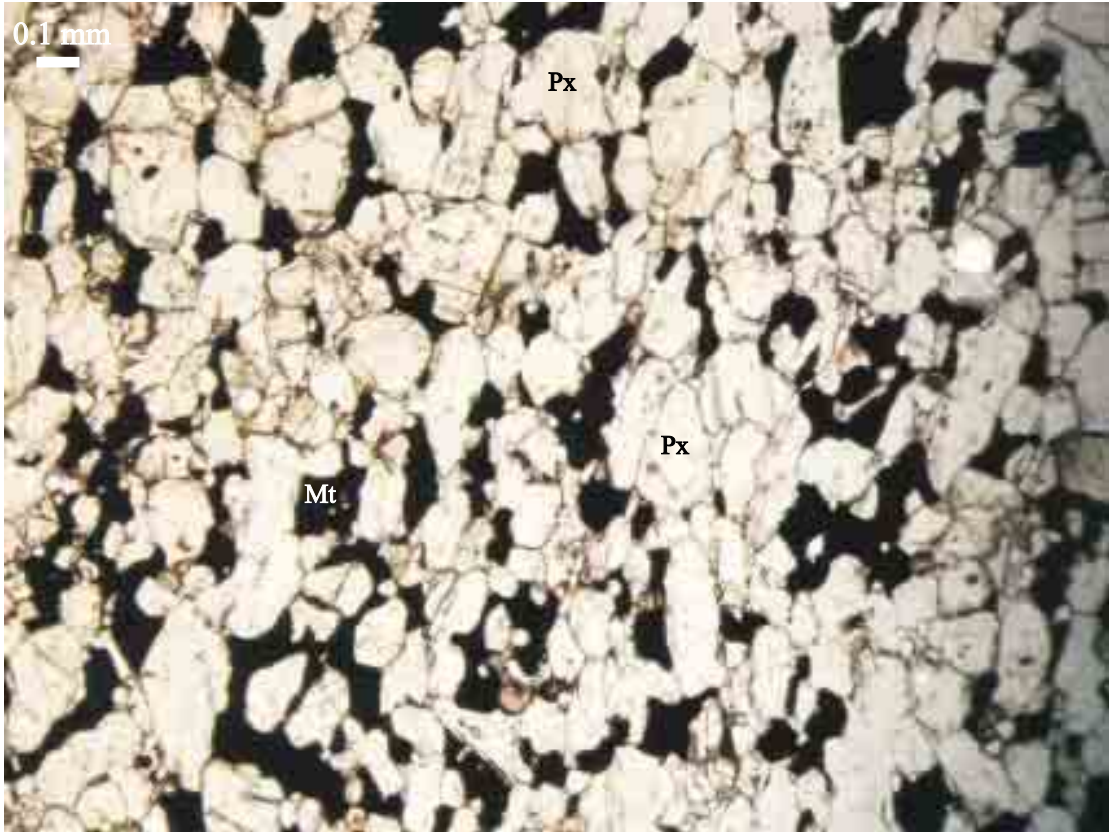


A



B

Figures 5C and 5D: Biotite-magnetite pyroxenite sample D-BMP-1. Pyroxenes show strong alignment and magnetite is an intercumulate phase. Labels are given in **Figure 5A** and **5B** caption.

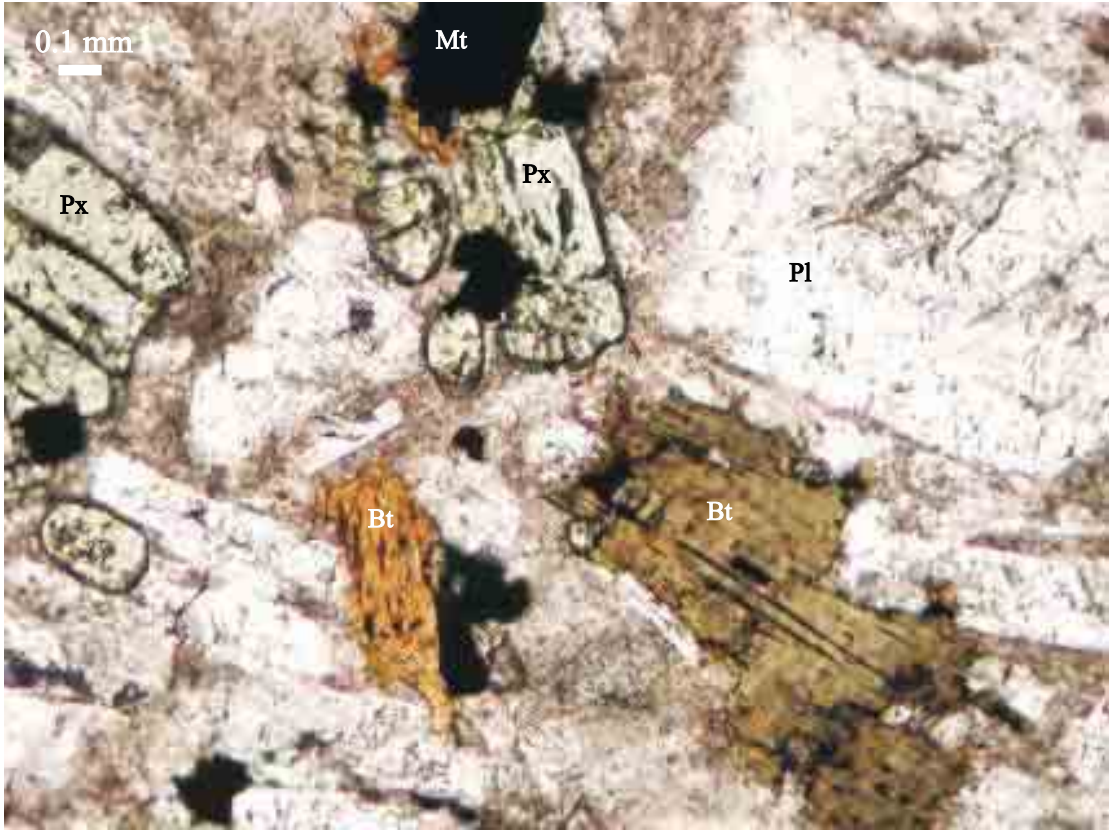


C

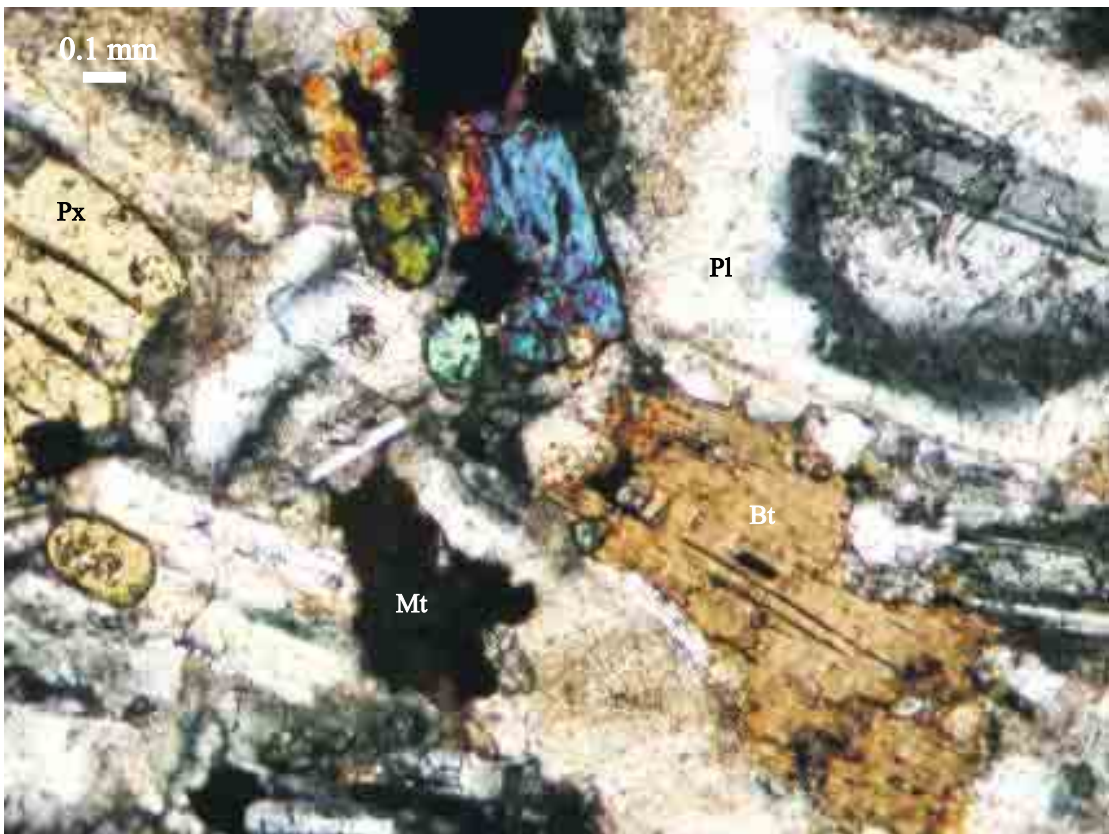


D

Figures 5E and 5F: Biotite-syeno-gabbro sample RK-3, dated for this study. Labels are given in **Figure 5a** and **5B** caption.



E

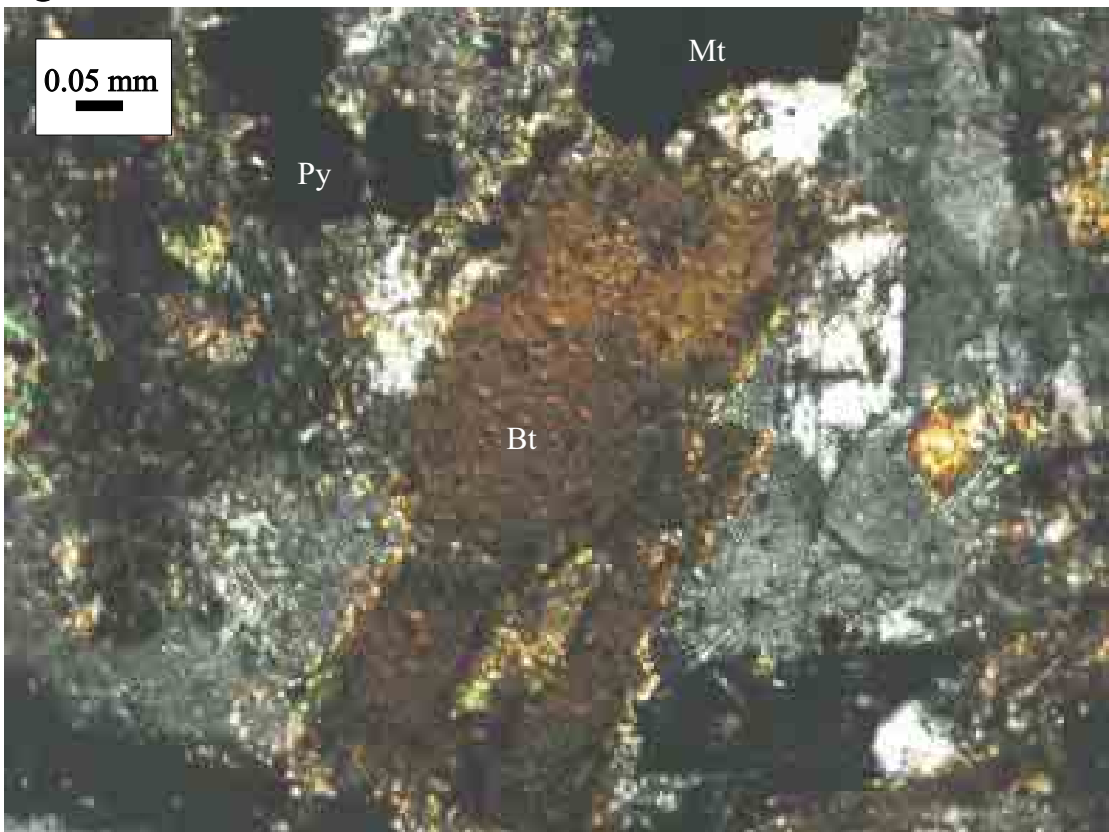


F

Figure 5G and 5H: Syenite sample PB-78, immediately adjacent in drill core to the dated sample PB-79. Labels are given in **Figure 5A** and **5B** caption.



G



H

Igneous rocks contemporaneous with ore

The dominant feature of the deposit area is the tonalite-granodiorite-quartz-monzonite porphyry (Kqmp) batholith adjacent to the Pebble deposit to the southwest. A zircon from this rock yielded an 89.7 ± 0.2 Ma U-Pb age (Bouley et al., 1995). This rock is porphyritic to equigranular, with quartz, plagioclase, K-feldspar, hornblende and accessory magnetite, sphene, zircon and apatite. Dikes thought to be comagmatic with the tonalite-granodiorite cut the biotite magnetite pyroxenite at depth. It has been interpreted that the porphyry suite is comagmatic with the tonalite-granodiorite (Bouley et al., 1995).

The porphyry suite, hydrothermal alteration and mineralization

The lithology logged and mapped as biotite diorite (Kbd) is known, through cross-cutting relationships, to be the oldest of the mineralized rocks at Pebble (Cominco unpublished report, 1994). It is known from several small dikes and has been so pervasively altered as to make identification of its pre-alteration lithology difficult. It may represent a potassically altered diorite (described above).

There are several variations of mineralized and altered granodiorite recognized in drill core at Pebble. There are equigranular (Kgde) and porphyritic (Kgdp) variations, with the porphyritic variety being more abundant and more closely correlated with high Cu grades (Bouley et al., 1995). Both contain quartz, primary K-feldspar and plagioclase largely altered to secondary K-feldspar, secondary biotite and local sericite. Relict albite twinning is visible on many of the altered plagioclase grains, and quartz phenocrysts are neomorphosed to fine grained quartz aggregates (Cominco annual report, 1993). Also recognized is a biotite granodiorite (Kgdb), but it is likely an altered textural variation of the Kgdp unit.

There are multiple examples of igneous breccias (Kibx) occurring as dikes and pipes in the deposit. Examples of both clast and matrix supported breccias have been found. The matrix of these bodies tends towards the composition of the granodiorites,

while the clasts are composed of all of the granodiorite lithologies (altered and unaltered), as well as hornfelsed sedimentary rocks. Examples can be found of all of the granodiorite lithologies grading into igneous breccias. They are variably mineralized and altered (Bouley et al., 1995).

The most noticeable and pervasive alteration facies at Pebble is potassic, as defined by secondary K-feldspar and/or biotite (Beane and Titley, 1981). Secondary biotite is common in the groundmass and as replacement of primary mafic minerals, and is usually associated with secondary rutile. Magmatic amphibole and biotite are generally replaced by shreddy aggregates of secondary greenish-brown biotite (Bouley et al., 1995). The more mafic lithologies affected by potassic alteration, such as the biotite diorite (Kbd), are almost entirely converted to secondary biotite with minor ferroan dolomite. The more common intermediate lithologies, such as the granodiorite series and the tonalite of the batholith, are dominated by secondary K-feldspar replacing magmatic plagioclase and orthoclase, and occurring as fine-grained masses in the matrix. Alteration biotite and K-feldspar also occur as veins with quartz in all porphyry lithologies. See Bouley, et al. (1995) for 2-D map distributions of biotite alteration, and Tracy (2001) for 3-D contours of biotite and K-feldspar alteration.

Phyllic alteration, as defined by alteration of host rocks to sericite + quartz (Beane and Titley, 1981), is not present as a pervasive alteration type within the ore deposit. However, north of the mineralized zone there is a small stock of barren rock pervasively altered to a quartz-sericite-pyrite unit (Kqsp). Other than quartz pseudomorphs after feldspar phenocrysts, the original texture of the rock has been destroyed and its pre-alteration composition is unknown. Within the mineralized zone, phyllic alteration is expressed as quartz veins with sericite selvages, and sericite is sometimes present as late stage disseminations, clots and as a partial replacement of K-feldspar. Additionally, argillic alteration is present mostly as a diffuse and discontinuous alteration facies at

Pebble, manifested as dusting of clay minerals on feldspars. Generally, phyllic and argillic alteration are underrepresented at Pebble relative to most Cu-porphyry deposits.

Propylitic alteration (secondary calcite+epidote±chlorite) affects a large area around the deposit, mostly within the diorite and the hornfelsed sedimentary rocks. Propylitic alteration occurs as far as 5 km south of Pebble, although it's not known whether this is related to the mineralized porphyry suite or to later intrusions.

There is a well-defined high grade core at Pebble, and an outline of the >0.2% Cu cutoff is shown on Figure 4. There has been a preliminary and moderately successful attempt to delineate “strong”, “moderate” and “weak” secondary biotite zones from visual inspection of drill core (Bouley et al., 1995). The “strong” zones correlate spatially to the highest grade portion of the deposit. Within this core, Cu mineralization commonly occurs as multiple stages of quartz-pyrite-chalcopyrite veins and veinlets, with chalcopyrite typically rimming pyrite. Generally, mineralization grades out from the core into disseminated pyrite and chalcopyrite. Molybdenum mineralization typically occurs as late quartz-molybdenite ± pyrite veins, often with sericite selvages, and almost always cutting potassic alteration. According to 3-dimensional geochemical modeling by Tracy (2001), high Au grades occur primarily within the higher grade Cu core, but are irregularly distributed. Bouley and others (1995) found that gold was almost always present as very small grains (several microns across) associated with pyrite and often near grain boundaries between pyrite and chalcopyrite.

Supergene enrichment of the Pebble deposit is spatially limited and not well-developed (Turner, personal communication). Locally, however, within the core of the deposit rocks may be oxidized to a depth of 240 meters (Bouley et al., 1995). Where enrichment is most well-developed, hypogene Cu-sulfides are completely replaced by pseudomorphs of digenite and lesser chalcocite. Overall, the supergene cap at Pebble does not add appreciably to its economic resource.

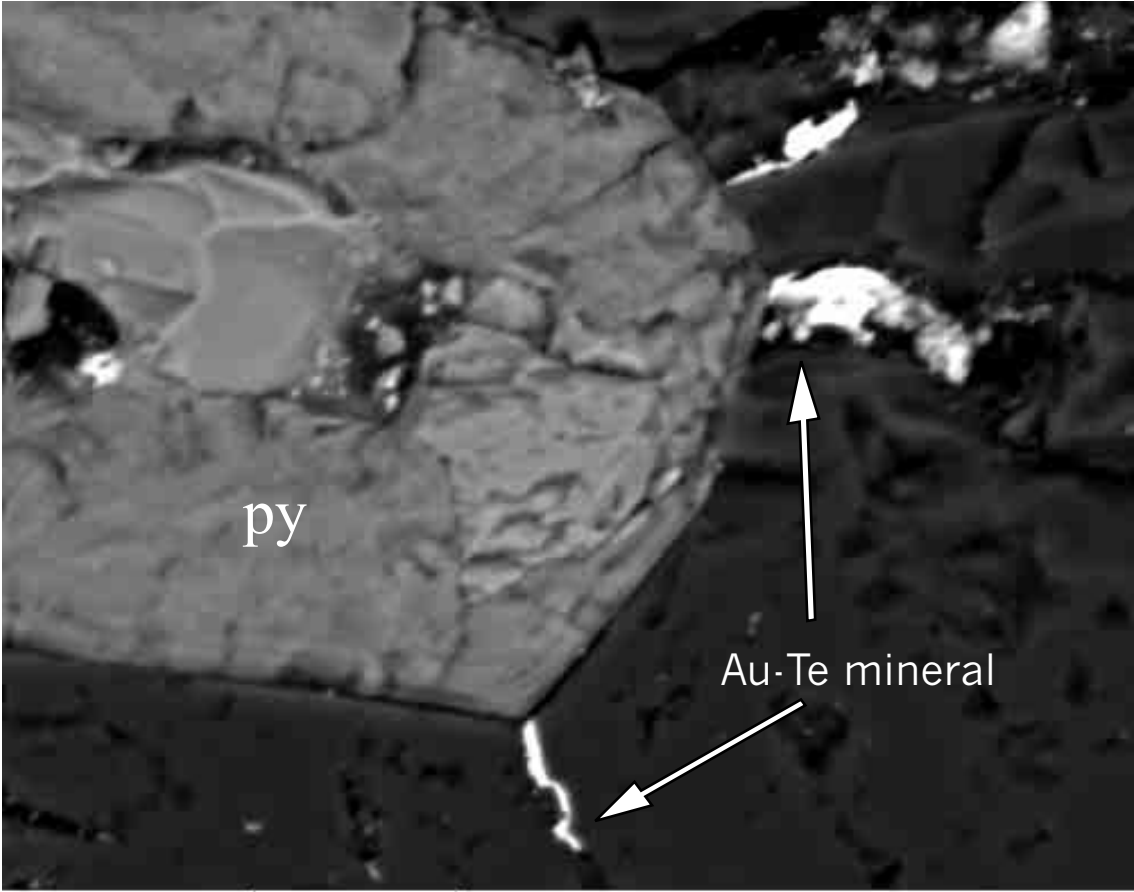
Post-ore rocks

South of the deposit are Cretaceous syenites (Ksy). These syenites generally have hypabyssal textures, and are composed of K-feldspar with lesser plagioclase, minor hornblende and biotite, both of which sometimes rim relict clinopyroxene crystals, and accessory apatite.

Pebble stocks are cut in several places by mafic Tertiary dikes, and the larger area is locally covered by Tertiary to Quaternary(?) basalt flows (Tb) and dacite tuffs (KTf). Although the dacite tuffs overlie and are thus younger than any dated Cretaceous rocks at Pebble, their precise age is unknown and they may be Tertiary, hence the Kef designation.

Approximately 4 km southeast of Pebble is Sill Mountain, a large accumulation of volcanic and hypabyssal latite (Tl). On the southern end of the surface exposure the Sill latite hosts the Sill epithermal Au-Ag prospect. A zircon from this body has yielded a U-Pb age of 46.2 ± 0.2 Ma (Bouley et al., 1995). The Sill latite typically contains K-feldspar and plagioclase in roughly subequal proportions and minor quartz, with hornblende and biotite. Drilling at Sill has revealed a variety of epithermal vein styles, including banded chalcedony veins, vuggy quartz veins, and veins with pseudomorphs of quartz after calcite. There are also rare K-feldspar-quartz veins which are cross-cut by the quartz veins whenever they have been found together. Sill contains locally high Au grades, most often associated with the banded veins of chalcedony. Several surface samples of altered latite contain visible gold, and electron micorprobe imaging and EDS analysis have revealed Au-telluride minerals spatially associated with pyrite (Figure 6). The vein style and metal endowment (precious metal rich and base metal poor) of Sill is indicative of an epithermal deposit. At the time of this writing, Sill is poorly understood. The known size of the deposit is small and no tonnage estimates are available.

Figure 6: Backscatter electron image from Sill sample S-122. A pyrite grain (py) is mantled by wispy Au-Te minerals (white in this image). This sample is of a banded chalcedony vein, and the matrix is quartz..



BE S-122a 10μm

SECTION 4

METHODS

Diamond drill logs and core were examined, and in some cases relogged, to sample altered and mineralized rocks from Pebble and Sill, and to sample pre- and post-mineralization igneous rocks. Samples were collected primarily from drill core housed in Iliamna, Alaska, with some nonmineralized samples collected from the surface of the Pebble deposit 30 kilometers to the northwest of Iliamna. All samples were examined at the University of Georgia, where a suite of samples was selected for further transmitted and reflective light petrography and electron microprobe study to determine their suitability for $^{40}\text{Ar}/^{39}\text{Ar}$ and Re-Os dating. In addition, neutron activation whole rock data from the Cominco American, Inc. annual report (1994) and a suite of ICP whole rock and ICP-MS trace element data from a suite of rocks selected for this study were examined. The ICP and ICP-MS analyses were run by Actlabs commercial laboratory in Tucson, Arizona, replicate analyses were provided to ensure accuracy, and analyses were calibrated using a variety of igneous rock, fly ash and iron metal standards. The location and specifics of the neutron activation analysis are unknown. Whole rock data were processed and CIPW norms were generated using Excel spreadsheets and Icpet 2000 software. Neutron activation data were normalized to 100% when loss on ignition (LOI) values were >3 weight percent.

All electron microprobe analyses were run on the University of Georgia's JEOL JXA-8600 superprobe calibrated with natural and synthetic mineral standards. Energy dispersive (EDS) analysis was used for mineral identification, and wavelength dispersive (WDS) quantitative analyses were run using an accelerating voltage of 15 kV, a beam current of 15 mA and beam diameters of 1-2 μm , except in the case of feldspars for

which 10 μm beam diameters were used. All corrections were carried out using standard Bence-Albee procedures.

All samples chosen for $^{40}\text{Ar}/^{39}\text{Ar}$ analysis were prepared at the University of Georgia except BJT-68, which was prepared at the University of Alaska, using standard magnetic and heavy liquid separation techniques. Rock samples were crushed to a 60 to 100 sieve size (250-150 μm). Minerals were picked by hand using a binocular microscope to ensure purity, and those samples containing carbonate were placed in dilute HCl overnight. All samples were irradiated along with standards in the uranium enriched research reactor of McMaster University in Hamilton, Ontario. All analyses were run at the Geochronology Laboratory at the University of Alaska Fairbanks, as described in York et al. (1981) and Layer et al. (1987). Samples were step-heated until fused using a 6-watt argon-ion laser and analyzed with a VG-3600 mass spectrometer. Argon isotope measurements were corrected for system blank and mass discrimination, as well as chlorine, calcium and potassium interference reactions as outlined in McDougall and Harrison (1999). All age steps, K/Cl and K/Ca steps are shown graphically on the spectra with $\pm 2\sigma$ errors (99% confidence level).

The sample chosen for molybdenite Re-Os geochronology was prepared and run at the Re-Os laboratory at Colorado State University, using procedures outlined in Stein et al. (1998a, 1998b). The molybdenite was separated, dissolved and equilibrated with Re and Os spikes in *aquia regia*. After recovery and purification, Os and Re were loaded onto Pt filaments and isotopic compositions were determined using NTIMS on a NBS 12-inch radius, 90° sector mass spectrometer.

Plateau and pseudo-plateau definition

Definition of and criteria for plateau ages were first described by Dalrymple and Lanphere (1974) as a means to provide more objective analysis of $^{40}\text{Ar}/^{39}\text{Ar}$ step-heating spectra. Since then, workers have proposed numerous schemes and definitions as to what

qualifies as a viable plateau (McDougall and Harrison, 1999). In this study, plateaus are defined using the following criteria:

- 1) a plateau is the portion of an age spectrum comprised of at least 50% of the total ^{39}Ar released, where
- 2) the apparent ages of the first and last steps are indistinguishable at the 2σ level,
- 3) any two adjacent steps are indistinguishable at the 1σ level,
- 4) the isochron age of the plateau steps is concordant with the weighted plateau age, and
- 5) where the $^{40}\text{Ar}/^{36}\text{Ar}$ of the plateau steps does not deviate significantly from the atmospheric value of 295.5.

These criteria are adapted from other worker's definitions, most notably from Lanphere and Dalrymple (1978) and Foland et al. (1986).

In this paper, the term pseudo-plateau is used to refer to a series of steps in a spectrum that do not meet the above criteria but which have been chosen at the expense of low temperature, high error steps that lie well outside the range of the remaining steps. Specifically, early steps which have a 1σ age error larger than 5%, and/or which lie outside of the 3σ error range of the subsequent step were excluded from the pseudo-plateau. While more meaningful than an integrated age, which includes all of the steps, the validity of a pseudo-plateau age will vary from sample to sample.

Isochrons are calculated, as outlined in MacDougall and Harrison (1999), therein referred to as "inverse isochrons". The $^{36}\text{Ar}/^{40}\text{Ar}$ of each step is plotted on the y-axis against its $^{39}\text{Ar}/^{40}\text{Ar}$ on the x-axis. An error is determined for each variable, resulting in ovoid points. A regression line is statistically determined, using both errors, and the x-intercept is proportional to the age of the sample. The y-intercept of the line is the initial trapped $^{36}\text{Ar}/^{40}\text{Ar}$ of the sample. The inverse of this value, the $^{40}\text{Ar}/^{36}\text{Ar}$, should be close to the atmospheric value of 295.5. Deviation from this value indicates trapped radiogenic argon. The MSWD (mean square of weighted deviates), a statistical measure of the fit of the line to the points, is determined for each isochron. Generally, MSWD values below

2.6 signify linearly correlated data, and the lower the value, the better the fit (i.e., a two point line has an MSWD of 0.0).

SECTION 5

GEOCHRONOLOGY SAMPLE DESCRIPTIONS

Sample S-91, (1 in Figure 3), is a vein K-feldspar from diamond drill hole S-19 at a depth of 449 feet (this and other drill core samples are hereon designated in the format S19, 449'; see appendix 3 for relevant drill hole locations and summary logs). The core sample is an altered latite (Tl) from the Sill epithermal Au-Ag deposit, dominated by fine grained quartz and containing ~2% pyrite by volume. It is located between two zones of epithermal veining: the zone above the sample is of mineralized banded chalcedony and the zone below is of barren vuggy quartz. The dated material is K-feldspar from a ~1 cm vein of K-feldspar + quartz, around which is a halo where both plagioclase and primary K-feldspar have been converted to aggregates of fine-grained secondary K-feldspar. The entire vein was excavated from the core and crushed to produce the K-feldspar mineral separate.

Samples RK-3 and BMP-7 are surface samples from ~4.5 km south of the Pebble main zone, (2 and 3, respectively, on Figure 3). Microphotographs of RK-3 are shown in Figure 5E-F. They are variations of the biotite-magnetite pyroxenite (Kbp) unit. Sample RK-3 is composed of partially weathered plagioclase from 0.5 to 2mm in length, sub- to euhedral diopside from 0.5 to 3 mm in length, biotite from very fine grained to 2 mm in length, blebby magnetite and minor pyrite. The minerals, primarily the plagioclase, diopside and biotite, show a weak but distinguishable alignment in thin section. RK-3 also contains a xenolith composed of 2-3 mm diopside and intercumulate magnetite. The outer edges of the xenolith are comprised of finer grained diopside, magnetite and minor biotite. BMP-7 contains less plagioclase than does RK-3, and it is finer grained. The biotite is generally larger, reaching lengths of 3.5 mm, and occurs as single grains and as clusters. Like RK-3, BMP-7 contains abundant magnetite. In addition to diopside, BMP-7

contains trace orthopyroxene (only one grain in the examined thin section). BMP-7 also contains fine-grained apatite. Microprobe work reveals that diopside and biotite in RK-3 and BMP-7 are of similar composition (appendix 1).

Sample PB-108 is a diorite found southwest of the Pebble main zone and adjacent to the biotite-pyroxenite body, in DDH PB24, 144'. It does not outcrop. The dominant primary minerals are plagioclase (An_{31-43}) and hornblende, very rare K-feldspar and accessory magnetite and apatite. This rock has been propylitically altered and contains secondary calcite, epidote and pyrite. Although some amphibole grains have been incipiently chloritized and epidotized, with the secondary minerals present as rims, microprobe work shows the grains to be hornblende (Deer, et al. 1966), and not actinolite as might be expected if the rock were more pervasively propylitized (see appendix 1 for microprobe analysis results). The hornblende grains were hand-picked carefully under a binocular microscope to avoid the most altered grains and placed in dilute HCl for more than twelve hours to remove any carbonate.

Sample PB-83 is from the hypogene center of the deposit, from DDH PB39, 169'. It was logged as a Kqmp (quartz monzonite porphyry). It is composed of fine-grained quartz, and the original feldspars are completely replaced by secondary K-feldspar. There is disseminated very fine-grained sericite throughout the groundmass, as well as pyrite and chalcopyrite. It contains a quartz-pyrite-chalcopyrite vein and a quartz-molybdenite vein with sericite selvages. It is the latter vein from which molybdenite was separated for Re-Os dating.

Sample BJT-68 is also from the hypogene zone of the Pebble deposit, from DDH PB28, 203'. It is a sample of mineralized igneous breccia (Kibx) containing fine grained quartz, secondary and primary K-feldspar, fine grained, shreddy secondary biotite in veins and disseminated, and very fine grained aggregates of sericite. It also contains pyrite, hematite and chalcopyrite. The biotite separated from this sample was a small aggregate excavated from a biotite-pyrite-chalcopyrite vein cutting through a 2.5 cm

primary K-feldspar grain. This grain was removed and crushed to extract the secondary biotite, thus avoiding any sericite overprint that was locally present in the groundmass.

Sample PB-162 is a biotite diorite (Kbd) from the main Pebble hypogene zone from DDH PB78, 193'. A K-feldspar-quartz-pyrite-chalcopyrite vein cuts this sample. The vein was extracted from the rock, crushed, and the K-feldspar was separated using heavy liquids and hand picking. A portion of the mineral separate was mounted and a point count using microprobe EDS analysis revealed it to be >80% pure K-feldspar, with the remainder being polyminerallic grains composed dominantly of quartz, K-feldspar with minor (<5%) albite.

Sample PB-79 (Figure 5G-H show photomicrographs of an immediately adjacent sample) is a hypabyssal syenite from the zone ~5 km south of the Pebble deposit, from DDH PB105, 74'. It is composed of K-feldspar with rare plagioclase, degraded clinopyroxene rimmed by hornblende and biotite, and primary biotite. The accessory minerals are apatite, ilmenite and minor pyrite. The primary biotite is the dated mineral from this rock.

SECTION 6

RESULTS

Geochronology

A summary of $^{40}\text{Ar}/^{39}\text{Ar}$ and Re-Os geochronologic results is presented in Table 1. Figure 7a-g contains age spectra, Ca/K spectra and Cl/K spectra for all $^{40}\text{Ar}/^{39}\text{Ar}$ analyses. Table 2 contains data from the Re-Os analysis of molybdenite from sample PB-83.

Four of the $^{40}\text{Ar}/^{39}\text{Ar}$ samples yielded good plateau ages. The vein K-feldspar sample PB-162 (Figure 7e), the igneous biotite sample PB-79 (Figure 7f) and the vein K-feldspar sample S-91 yield pseudo-plateau ages. PB-162 shows a saddle-shaped spectrum with an apparent argon gain on the first step and two higher temperature steps just outside of the 1σ error of an adjacent step. Only the first step is excluded to generate a pseudo-plateau. PB-79 yielded a more disturbed spectrum, and the first two steps are excluded to generate a pseudo-plateau. The Ca/K spectrum for PB-79 is somewhat complex, but it should be noted that the age spectra shows an inverse relationship to the Ca/K spectra, in that the age steps decrease when Ca/K increases. This probably indicates the presence of another phase in the mineral separate with more Ca than biotite, possibly amphibole or epidote, present as inclusions or as rims on the biotite. This other phase is either slightly younger or its replacement of biotite has caused minor Ar loss in some crystal domains.

S-91 is the only sample where the isochron age is interpreted as the age most likely to be accurate. The difference between the pseudo-plateau age and the whole isochron age is small but significant at 46.6 ± 0.1 Ma versus 46.1 ± 0.2 Ma, respectively. The isochron age was chosen because of the indication of excess argon (initial $^{40}\text{Ar}/^{36}\text{Ar}$ of 302.7 ± 1.5 compared to the atmospheric ratio of 295.5) and the excellent fit of the line on the isochron diagram (MSWD of 1.11).

Table 2: Re-Os age for molybdenite from the Pebble Cu-Au porphyry deposit, Lake Iliamna, SW Alaska ⁵

Pebble Deposit	AIRIE Run	Re (ppm) ¹	¹⁸⁷ Re (ppm) ¹	¹⁸⁷ Os (ppb) ₁	Age (Ma) ^{2, 3, 4}
Drill Hole PB-39 169'	CT-138	2070 (2)	1301 (1)	1941 (3)	89.5 ± 0.3
CS98-PB83					

¹ Re and ¹⁸⁷Os uncertainties in parentheses are absolute at 2σ uncertainty for the last digit indicated.

² Uncertainties include error in (1) ¹⁸⁵Re and ¹⁹⁰Os spike calibrations, 0.05% and 0.15%, respectively,

(2) magnification with spiking, (3) mass spectrometric measurement of isotopic ratios, and (4) the ¹⁸⁷Re decay constant (0.31%).

³ Molybdenites rarely require a blank correction. In the AIRIE molybdenite laboratory, blanks are

Re = 17-18 pg, Os = 6-8 pg with a variable ¹⁸⁷Os/¹⁸⁸Os ranging from 0.5 to 8.3.

⁴ Age is calculated by $^{187}\text{Os} = ^{187}\text{Re} (e^{\lambda t} - 1)$ where $\lambda = ^{187}\text{Re}$ decay constant and t = age; ¹⁸⁷Re decay

constant used is $1.666 \times 10^{-11} \text{ yr}^{-1}$ with an uncertainty of 0.31 % (Smoliar et al., 1996); uncertainty

shown for age is absolute at 2σ.

⁵ from Holly Stein at AIRIE, Colorado State University, Fort Collins, Colorado

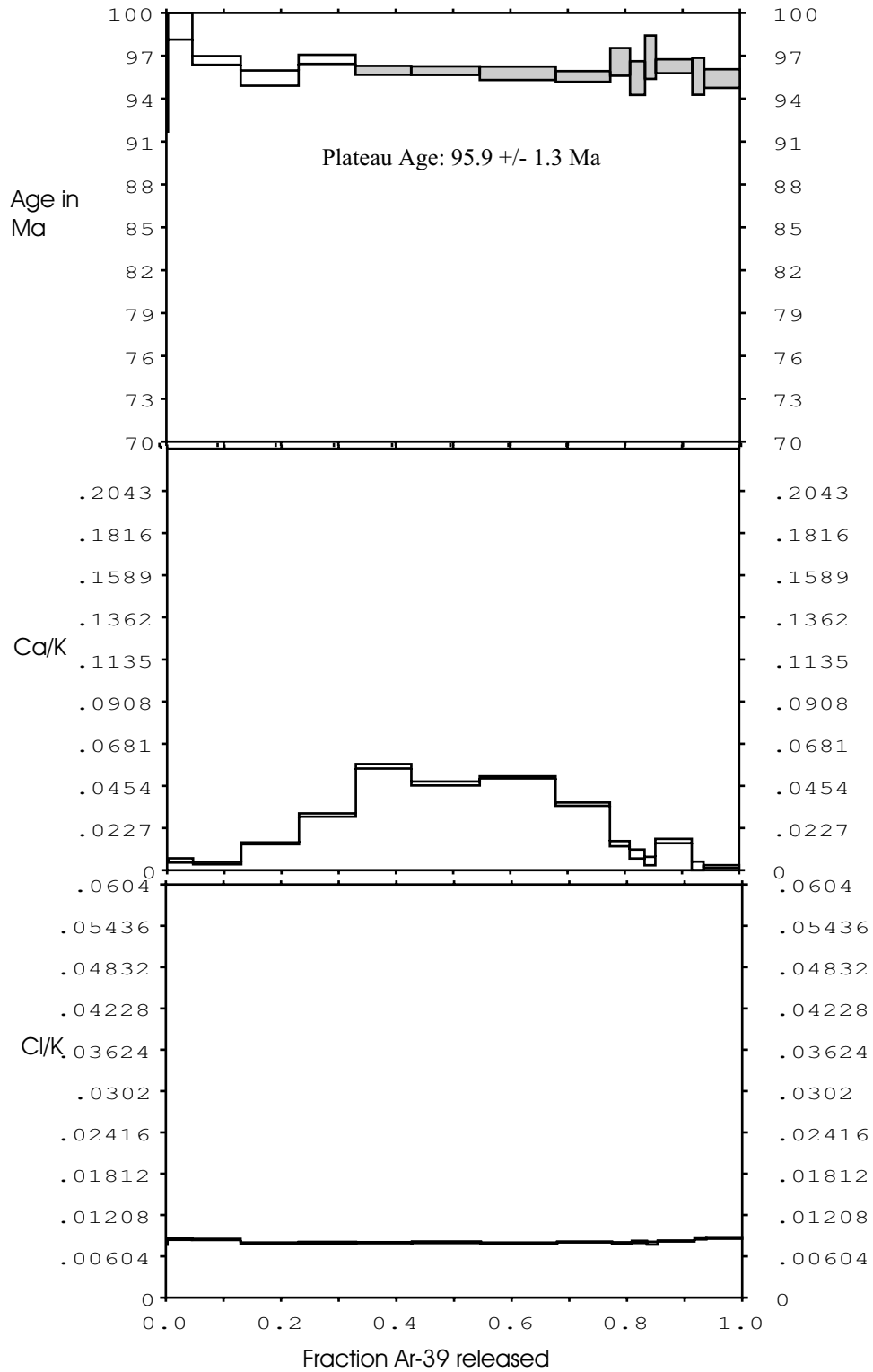


Figure 7a
 BMP-7:
 igneous biotite from Kbp

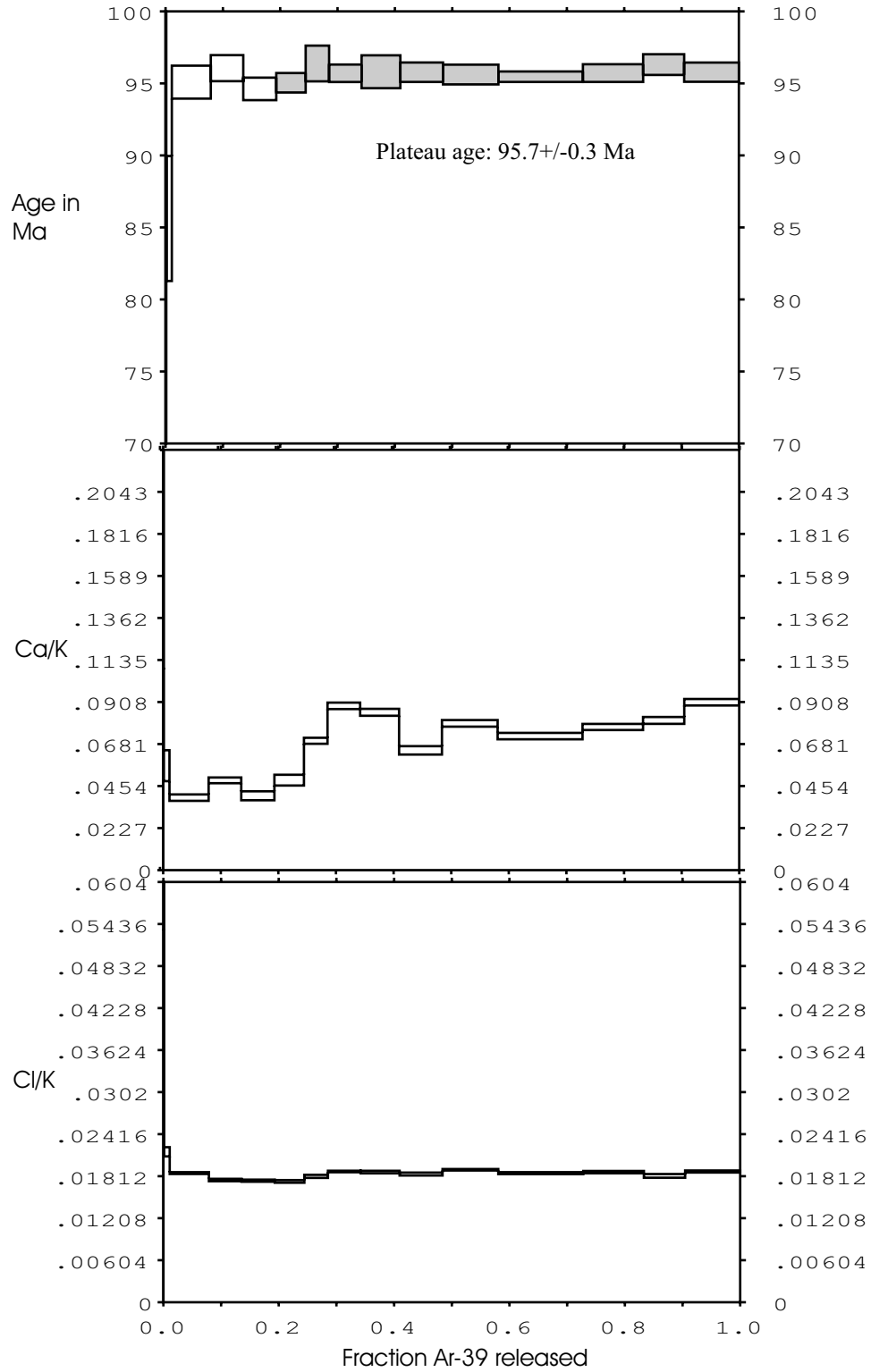


Figure 7b
 RK-3:
 igneous biotite in Kbp

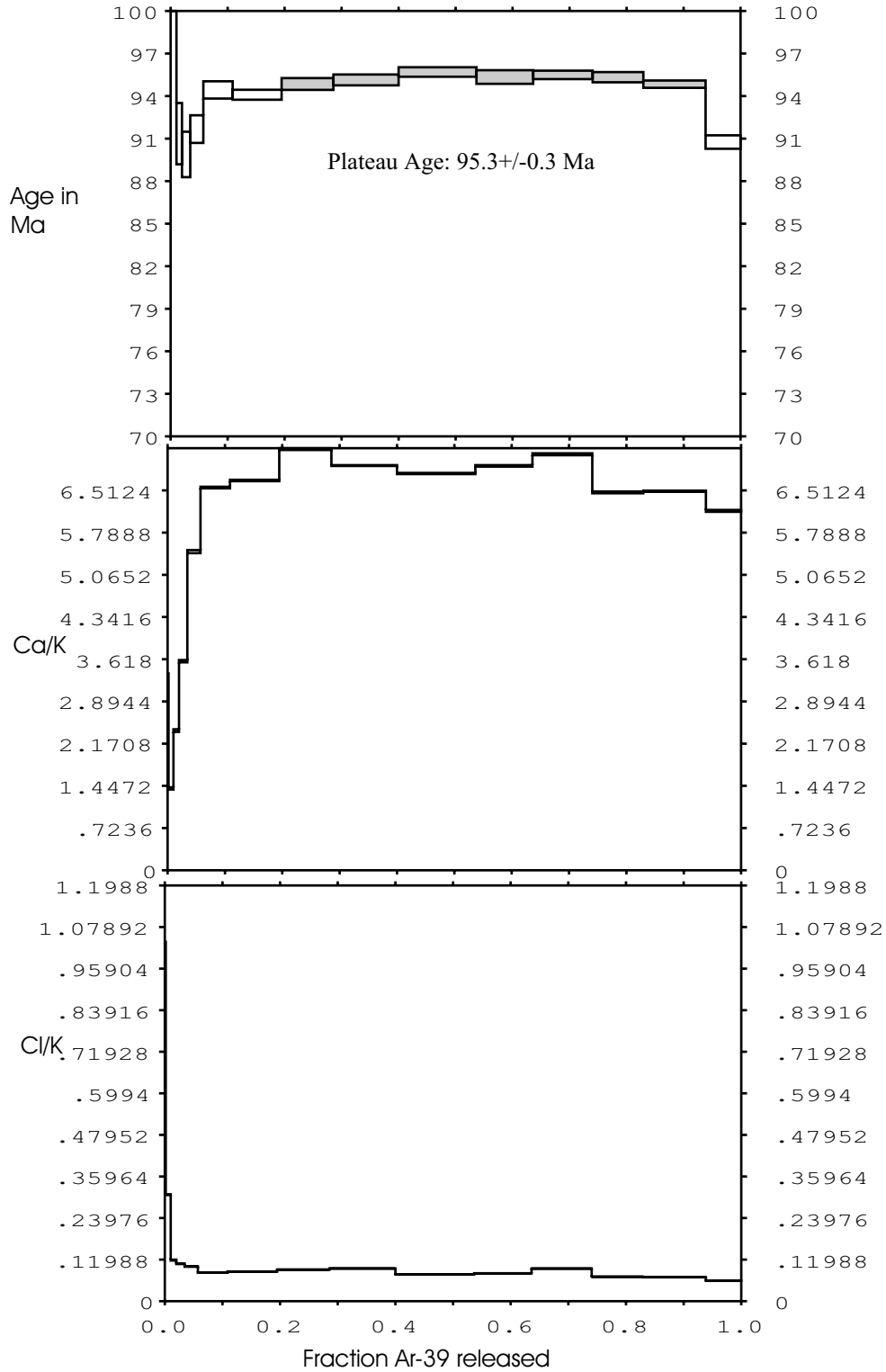


Figure 7c
 PB-108:
 igneous hornblende in Kd

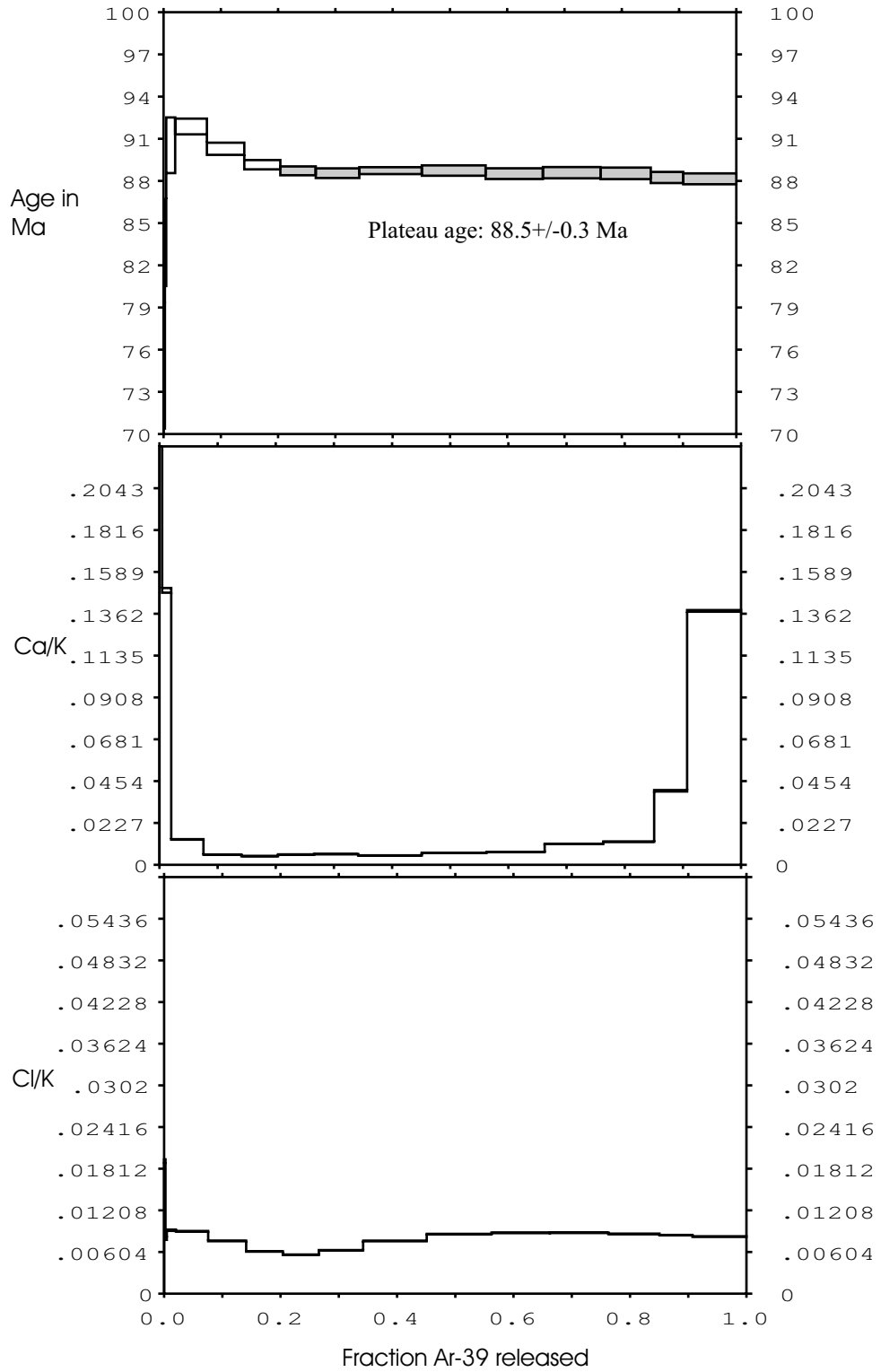


Figure 7d
 BJT-68:
 hydrothermal biotite in Kibx

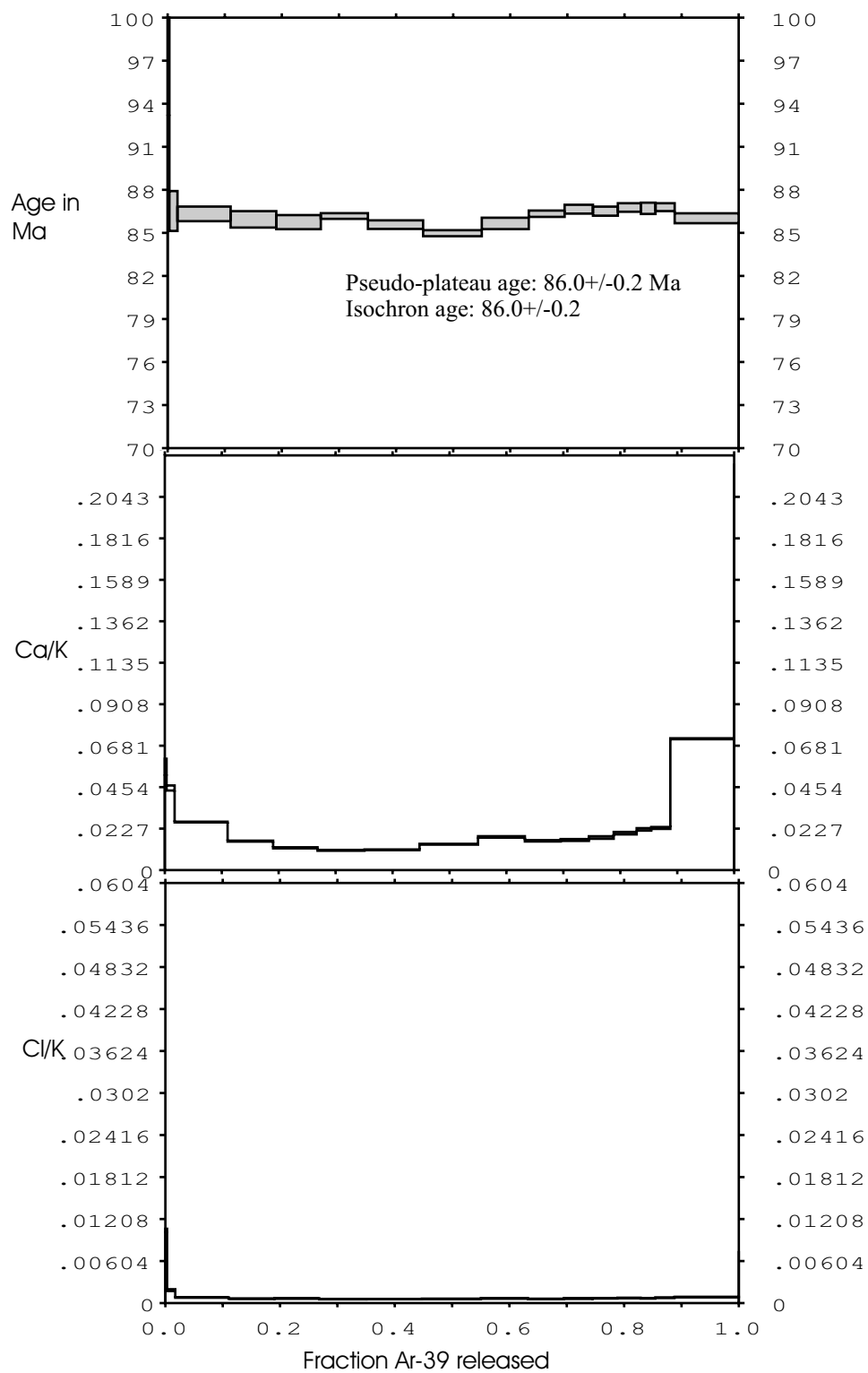


Figure 7e
 PB-162:
 hydrothermal K-feldspar in Kbd

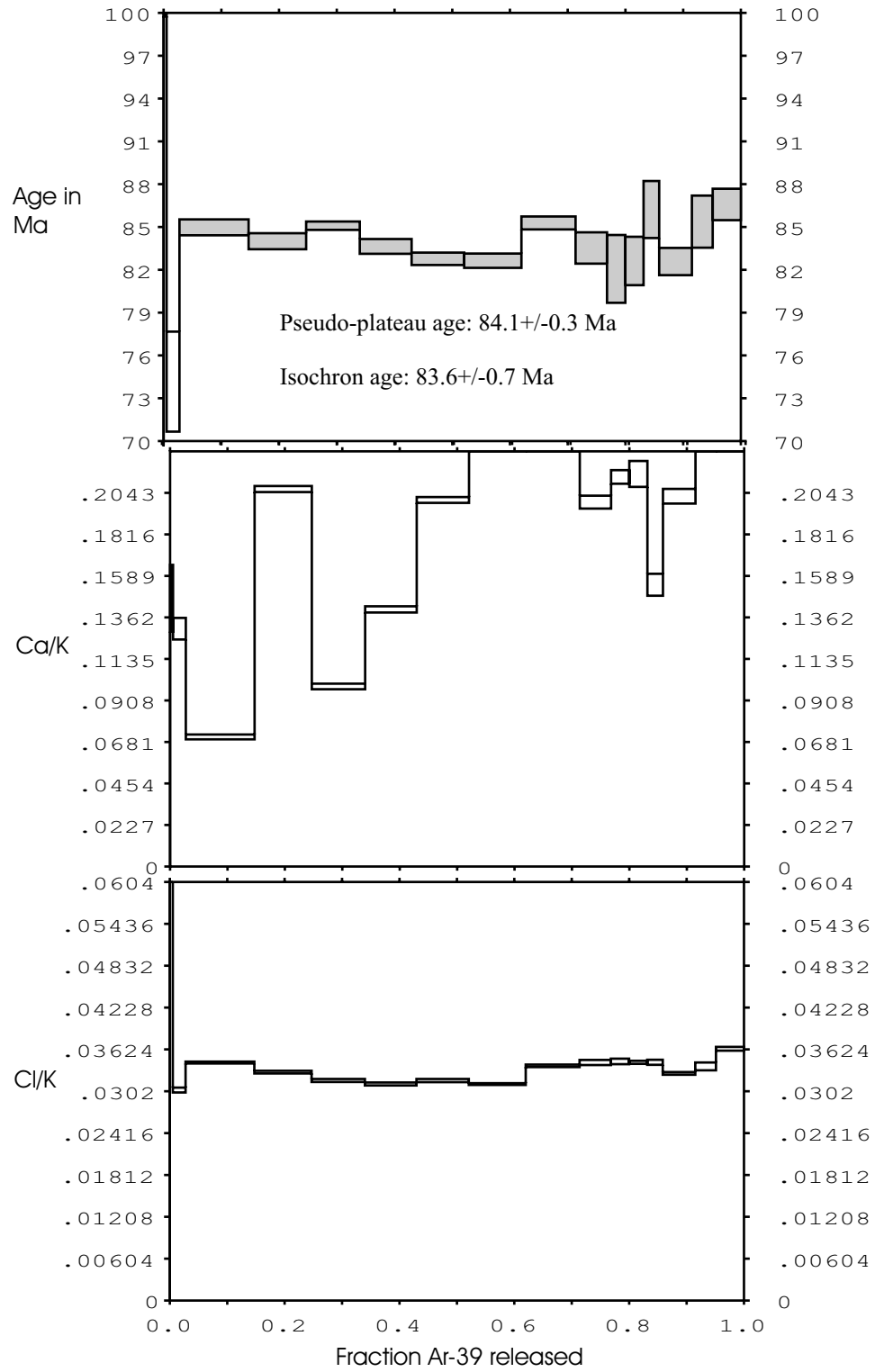


Figure 7f
 PB-79:
 igneous biotite in Ksy

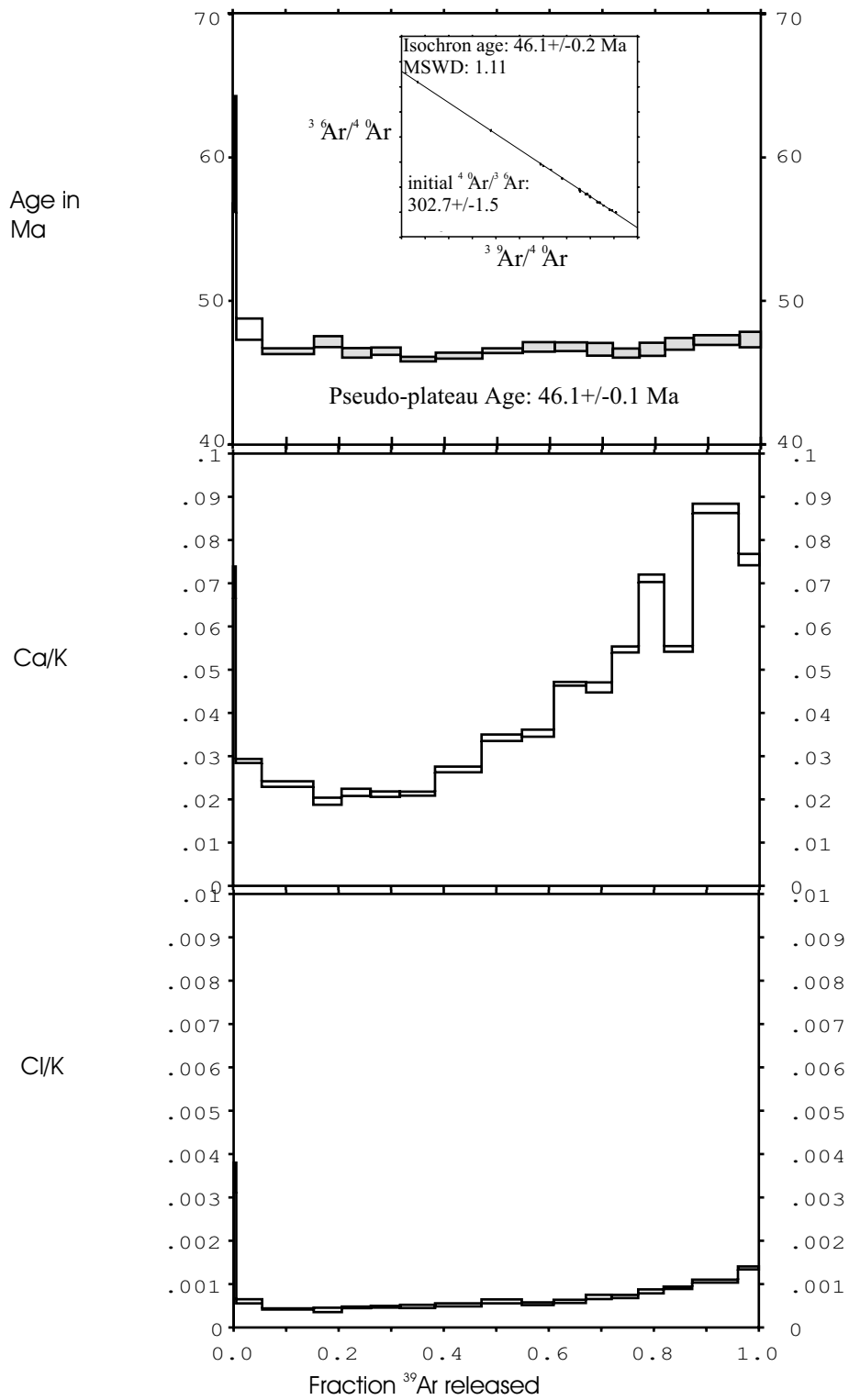


Figure 7g
S-91:
hydrothermal K-feldspar in Tl

Sample PB-108 (Figure 7c) has a humped age spectra with a last step as young as the early, high-error steps. While this could possibly indicate excess argon or an otherwise complex thermal history, hornblendes are known for their sometimes enigmatic patterns, probably due to the complexity of their crystal solid solution (McDougall and Harrison, 1999). The plateau is concordant with the isochron age and comprises 74.4% of the total ^{39}Ar released, and is likely an accurate age.

Geochemistry

Two sets of geochemical data are used in this study. The first is a series of whole rock neutron activation data from Cominco American, Inc., previously examined by Bouley et al. (1995), along with CIPW norms (Table 3). These data are representative of samples of lithologies from the deposit and immediate area. The rock types are those described in previous sections. The second data set contains ICP-MS whole rock and trace element data, including rare earth elements and CIPW norms, for samples selected specifically for this study (Table 4).

Table 3: Whole rock geochemical data and CIPW norms for Pebble lithologies

sample	GAB1	GAB2	GAB3	GAB4	GAB5	DIO1	DIO2	DIO3	BP1
lith code	Kgb	Kgb	Kgb	Kgb	Kgb	Kd	Kd	Kd	Kbp
SiO2	48.83	51.83	50.72	49.78	50.66	49.47	52.25	53.07	60.49
Al2O3	20.08	20.59	19.93	19.94	20.22	18.46	19.11	20.24	19.21
Fe2O3	1.45	1.06	1.13	1.13	1.01	1.7	1.23	1.08	4.04
FeO	10.14	7.42	7.93	7.91	7.05	11.89	8.61	7.59	2.74
MgO	4.07	4.45	4.93	5.37	5.67	4.34	4.59	4.34	2.55
CaO	2.01	1.96	3.13	3.72	3.43	2.41	3.38	2.83	2.58
Na2O	6.31	5.82	6.08	6.31	6	3.87	4.65	5.36	3.66
K2O	5.82	5.58	4.92	4.52	4.66	6.81	5.05	4.41	3.22
TiO2	0.71	0.73	0.75	0.77	0.78	0.63	0.62	0.65	0.98
P2O5	0.53	0.51	0.45	0.52	0.49	0.4	0.47	0.4	0.47
MnO	0.06	0.05	0.03	0.03	0.04	0.03	0.03	0.03	0.05
LOI									
Total	*100.01	*100.00	*100.00	*100.00	*100.01	*100.01	*99.99	*100.00	*100.00
Q	-	-	-	-	-	-	-	-	18.8
or	34.39	32.97	29.07	26.71	27.54	40.24	29.84	26.06	19.03
ab	10.37	22.83	17.81	15.65	18.59	9.18	24.92	32.49	30.97
an	6.51	6.39	12.56	12.73	13.82	9.34	13.7	11.43	9.73
lc	-	-	-	-	-	-	-	-	-
ne	23.31	14.31	18.22	20.44	17.43	12.77	7.81	6.97	-
kal	-	-	-	-	-	-	-	-	-
C	1.01	2.63	-	-	0.24	1.3	0.97	2.46	6.14
di	-	-	0.02	1.92	-	-	-	-	-
hy	-	-	-	-	-	-	-	-	6.52
wo	-	-	-	-	-	-	-	-	-
ol	19.74	16.75	18.21	18.23	18.31	22.59	18.69	16.86	-
ac	-	-	-	-	-	-	-	-	-
mt	2.1	1.54	1.64	1.64	1.46	2.46	1.78	1.57	5.86
il	1.35	1.39	1.42	1.46	1.48	1.2	1.18	1.23	1.86
hem	-	-	-	-	-	-	-	-	-
ap	1.23	1.18	1.04	1.2	1.14	0.93	1.09	0.93	1.09
tn	-	-	-	-	-	-	-	-	-
CS	-	-	-	-	-	-	-	-	-
An	38.6	21.9	41.4	44.9	42.6	50.4	35.5	26	23.9
Total	100	100	100	100	100	100	100	100	100

* indicates analyses normalized to 100 wt. %

Table 3, cont.: Whole rock geochemical data and CIPW norms for Pebble lithologies

sample	BP2	BP3	BP4	BPF1	BPF3	BPF4	Syenite1	Syenite2	Syenite3	Syenite4
lith code	Kbp	Kbp	Kbp	Kbp	Kbp	Kbp	Ksy	Ksy	Ksy	Ksy
SiO2	56.31	38.49	40.37	58.62	59.18	49.47	51.40	59.21	60.47	58.46
Al2O3	16.08	5.13	18.52	19.08	17.96	14.97	18.31	19.26	19.64	18.59
Fe2O3	4.20	2.34	1.4	3.48	3.49	8.23	5.15	3.04	2.39	3.26
FeO	5.32	16.37	9.81	1.56	2.77	7.60	3.40	1.63	1.24	1.80
MgO	3.75	17.13	8.97	1.58	2.32	6.16	3.96	1.30	0.80	1.69
CaO	3.62	18.28	11.53	4.44	5.21	8.42	8.50	3.54	2.46	3.01
Na2O	3.95	0.96	4.06	4.96	4.44	1.53	3.80	5.25	5.63	3.87
K2O	3.99	0.11	3.5	5.28	3.39	1.59	3.64	5.76	6.47	8.18
TiO2	1.99	0.91	0.82	0.53	0.71	1.01	0.95	0.53	0.50	0.61
P2O5	0.62	0.0	0.89	0.36	0.42	0.74	0.69	0.36	0.29	0.39
MnO	0.16	0.28	0.14	0.12	0.10	0.26	0.19	0.12	0.10	0.13
LOI										
Total	*100.00	*100.00	*100.01	*100.00	*100.00	*100.00	*100.00	*100.00	*100.00	*100.00
Q	4.16	-	-	-	5.82	1.82	-	-	-	-
or	23.58	-	-	31.2	20.03	9.4	21.51	34.04	38.23	48.34
ab	33.42	-	-	41.56	37.57	12.95	23.69	42.04	43.03	27.88
an	13.91	9.36	21.97	14.2	19.06	29.28	22.15	11.98	9.21	9.19
lc	-	0.51	16.22	-	-	-	-	-	-	-
ne	-	4.4	18.61	0.22	-	-	4.58	1.29	2.5	2.64
kal	-	-	-	-	-	-	-	-	-	-
C	0.17	-	-	-	-	-	-	-	-	-
di	-	17.27	2.37	4.48	3.31	6.39	12.71	2.65	0.88	2.6
hy	14.41	-	-	-	8.54	32.3	-	-	-	-
wo	-	-	-	-	-	-	-	-	-	-
ol	-	44.72	26.98	3.41	-	-	8.11	3.12	1.58	4.1
ac	-	-	-	-	-	-	-	-	-	-
mt	5.06	3.39	2.03	2.94	3.2	3.64	3.55	2.94	2.9	3.06
il	3.78	1.73	1.56	1.01	1.35	1.92	1.8	1.01	0.95	1.16
hem	-	-	-	-	-	-	-	-	-	-
ap	1.44	-	2.06	0.83	0.97	1.71	1.6	0.83	0.67	0.9
tn	-	-	-	-	-	-	-	-	-	-
CS	-	18.62	8.21	-	-	-	-	-	-	-
An	29.4	100	100	25.5	33.7	69.3	48.3	22.2	17.6	24.8
Total	99.9	100	100	99.9	99.9	99.4	99.7	99.9	100	99.9

* indicates analyses normalized to 100 wt. %

Table 3, cont.: Whole rock geochemical data and CIPW norms for Pebble lithologies

sample	Syenite5	GranE	GranLk	GranW1	GranW2	GranW3	Latite1	Latite2	Latite3	Latite4	Tbasalt	Tdacite
lith code	Ksy	-	-	-	-	-	Tl	Tl	Tl	Tl	Tb	Ta
SiO2	58.00	64.19	62.37	63.25	62.67	62.56	62.15	67.83	68.68	67.4	48.35	54.46
Al2O3	18.64	17.21	17.05	16.36	16.52	16.86	15.89	15.17	15.11	15.26	15.94	17.37
Fe2O3	3.18	2.8264	3.3975	3.0564	3.203	2.57	1.91	1.59	1.31	2.26	3.5432	4.2792
FeO	2.32	1.38	1.28	1.56	1.68	2.45	3.6	1.58	1.73	1.01	6.53	2.79
MgO	1.84	1.25	1.24	1.54	1.71	1.46	1.66	0.72	0.58	0.61	7.03	3.72
CaO	5.34	4.6	4.27	4.82	5.02	5.2	3.74	1.8	1.37	1.82	10.15	7.24
Na2O	5.20	4.13	4.01	3.84	3.81	3.67	4.09	4.54	4.62	3.99	3.94	3.94
K2O	4.36	3.15	3.32	3.25	3.17	2.78	2.57	3.99	4.21	3.94	1.17	2
TiO2	0.60	0.46	0.49	0.48	0.52	0.56	0.96	0.45	0.41	0.54	1.57	0.95
P2O5	0.38	0.28	0.35	0.39	0.39	0.23	0.36	0.14	0.09	0.13	0.31	0.54
MnO	0.15	0.12	0.1	0.13	0.14	0.13	0.18	0.12	0.1	0.11	0.18	0.14
LOI		1.02	1.82	0.63	0.83						1.17	1.9
Total	*100.00	100.62	99.70	99.31	99.66	98.47	97.11	97.93	98.21	97.07	99.88	99.33
Q	-	17.59	16.37	17.72	16.98	17.78	17.33	21.13	21.42	24.67	-	6.08
or	25.77	18.61	19.62	19.21	18.73	16.43	15.19	23.58	24.88	23.28	6.91	11.82
ab	42.95	34.95	33.93	32.49	32.24	31.05	34.61	38.42	39.09	33.76	24.82	33.34
an	14.64	19.12	18.72	17.8	18.61	21.32	16.2	8.02	6.21	8.18	22.35	23.8
lc	-	-	-	-	-	-	-	-	-	-	-	-
ne	0.57	-	-	-	-	-	-	-	-	-	4.62	-
kal	-	-	-	-	-	-	-	-	-	-	-	-
C	-	-	-	-	-	-	0.44	0.45	0.68	1.43	-	-
di	7.69	1.46	0.14	2.77	2.91	2.4	-	-	-	-	20.89	6.71
hy	-	2.44	3.02	2.55	2.91	4.17	7.92	2.86	3.05	1.52	-	6.42
wo	-	-	-	-	-	-	-	-	-	-	-	-
ol	3.22	-	-	-	-	-	-	-	-	-	10.29	-
ac	-	-	-	-	-	-	-	-	-	-	-	-
mt	3.04	3.51	3.03	4.06	4.36	3.73	2.77	2.31	1.9	2.05	5.13	6.21
il	1.14	0.87	0.93	0.91	0.99	1.06	1.82	0.85	0.78	1.03	2.98	1.8
hem	-	0.41	1.31	0.26	0.19	-	-	-	-	0.85	-	-
ap	0.88	0.65	0.81	0.9	0.9	0.53	0.83	0.32	0.21	0.3	0.72	1.25
tn	-	-	-	-	-	-	-	-	-	-	-	-
CS	-	-	-	-	-	-	-	-	-	-	-	-
An	25.4	35.4	35.6	35.4	36.6	40.7	31.9	17.3	13.7	19.5	47.4	41.7
Total	99.9	99.6	97.9	98.7	98.8	98.5	97.1	97.9	98.2	97.1	98.7	97.4

* indicates analyses normalized to 100 wt. %

Table 4: ICP-MS whole rock and trace element geochemical data and CIPW norms for selected Pebble samples

sample	CS98-PB108	CS98-DSY2	CS98-PB141	CS98-PB5	CS98-BMP3	CS98-DBMP1	CS98-PB78	CS98-GAB1
lith code	Kd	Kbp	Kbp	Kgb	Kbp	Kbp	Ksy	Kgb
SiO2	59.74	55.79	35.60	53.39	55.04	35.30	52.90	53.80
Al2O3	17.13	17.82	4.74	17.28	16.58	4.09	17.55	17.25
Fe2O3	5.77	6.63	24.79	10.47	7.87	26.27	8.54	9.64
MnO	0.114	0.171	0.364	0.174	0.149	0.270	0.209	0.123
MgO	1.78	2.33	10.18	4.85	3.17	10.37	3.39	3.31
CaO	5.75	6.51	18.13	3.30	7.04	19.81	4.91	7.84
Na2O	3.97	4.76	0.41	3.04	4.16	0.31	2.20	3.27
K2O	3.52	3.59	0.56	1.88	3.97	0.03	7.51	2.05
TiO2	0.597	0.635	1.474	0.985	0.626	1.518	0.620	0.863
P2O5	0.31	0.38	1.71	0.51	0.54	2.67	0.58	0.48
LOI	1.73	0.98	1.23	3.23	0.43	0.00	1.88	0.93
TOTAL	100.41	99.58	99.18	99.11	99.56	100.46	100.29	99.54
Sc	13	10	55	22	15	68	13	16
V	142	175	677	220	210	729	191	195
Cr	0	0	0	95	0	0	26	31
Co	8	11	44	4	16	71	15	10
Ni	0	21	43	45	0	46	0	69
Cu	67	99	57	23	48	34	96	50
Zn	164	123	376	63	92	143	95	55
Ga	19	19	17	21	18	17	16	17
Ge	2	2	3	2	2	3	2	2
As	0	0	31	0	0	5	16	0
Rb	64	69	18	64	72	0	120	51
Sr	1060	1490	421	439	1630	481	1460	843
Y	20	20	23	21	17	24	17	22
Zr	111	93	44	99	79	24	67	103
Nb	11	6	0	7	6	0	4	11
Sb	0.6	0.0	2.9	0.0	0.0	0.8	1.9	1.0
Cs	1.2	1.6	2.3	7.5	1.7	0.0	4.2	2.0
Ba	763	604	53	297	630	12	985	284
La	18.3	20.4	16.7	12.5	19.8	16.7	14.8	17.0
Ce	34.2	39.9	40.1	25.9	38.5	39.6	30.1	34.4
Pr	4.28	5.29	6.34	3.53	5.09	6.36	4.04	4.53
Nd	16.4	21.5	30.7	14.7	20.5	31.1	16.9	18.5
Sm	3.6	4.3	7.7	3.6	4.4	8.1	3.9	4.2
Eu	1.23	1.51	2.54	1.31	1.45	2.69	1.28	1.44
Gd	3.5	4.1	7.6	3.6	4.0	8.0	3.7	4.0
Tb	0.6	0.6	1.0	0.6	0.6	1.1	0.6	0.7
Dy	3.5	3.6	5.1	3.8	3.1	5.2	3.2	3.9
Ho	0.7	0.7	0.9	0.8	0.6	0.9	0.6	0.8
Er	2.1	2.0	2.1	2.3	1.7	2.1	1.7	2.2
Tm	0.32	0.30	0.25	0.35	0.25	0.24	0.26	0.34
Yb	2.1	2.0	1.7	2.2	1.6	1.5	1.7	2.2
Lu	0.33	0.30	0.24	0.33	0.25	0.21	0.25	0.34
Hf	2.8	2.5	2.0	2.8	2.1	1.3	1.8	2.7
Ta	1.0	0.8	0.1	0.6	0.6	0.0	0.4	1.0
Tl	0.3	0.2	0.3	1.5	0.2	0.0	1.6	0.6
Pb	8	15	32	7	11	0	33	0
Th	3.0	2.7	0.6	2.0	2.3	0.5	2.9	2.2
U	1.7	1.8	0.4	1.4	1.2	0.1	1.4	1.1

Table 4: ICP-MS whole rock and trace element geochemical data and CIPW norms for selected Pebble samples

sample	CS98- PB108	CS98-DSY2	CS98- PB141	CS98-PB5	CS98-BMP3	CS98- DBMP1	CS98-PB78	CS98-GAB1
lith code	Kd	Kbp	Kbp	Kgb	Kbp	Kbp	Ksy	Kgb
Q	9.19	-	-	11.18	-	-	-	4.55
or	20.8	21.21	-	11.11	23.46	-	44.38	12.11
ab	33.59	40.28	-	25.72	35.05	-	15.54	27.67
an	18.52	16.65	9.44	13.04	14.84	9.68	15.83	26.34
lc	-	-	2.59	-	-	0.14	-	-
ne	-	-	1.88	-	0.08	1.42	1.67	-
kal	-	-	-	-	-	-	-	-
C	-	-	-	5.47	-	-	-	-
di	6.55	10.83	26.93	-	13.64	28.25	3.92	7.82
hy	4.75	0.20	-	21.89	-	-	-	13.24
wo	-	-	-	-	-	-	-	-
ol	-	3.80	32.40	-	5.96	33.82	10.84	-
ac	-	-	-	-	-	-	-	-
mt	3.04	3.10	4.31	3.61	3.09	4.38	3.07	3.42
il	1.14	1.22	2.79	1.88	1.20	2.89	1.18	1.63
hem	-	-	-	-	-	-	-	-
ap	0.72	0.88	3.96	1.18	1.25	6.19	1.34	1.11
CS	-	-	11.46	-	-	11.55	-	-
An	35.5	29.3	100	33.6	29.8	100	50.5	48.8
Total	98.3	98.2	95.8	95.1	98.6	98.3	97.8	97.9

SECTION 7

DISCUSSION

Geochronology

White and Heropoulos (1986) reported that modern analogues to near surface hydrothermal systems last on the order of ten thousand to two hundred thousand years. Norton and Knight (1977) used numerical modeling to demonstrate that the cooling of a single intrusion is expedited by hydrothermal circulation, and that even large bodies will only sustain hydrothermal circulation for tens to hundreds of thousands of years. Field and geochronologic studies of single hydrothermal systems related to porphyry and epithermal mineralization generally cannot resolve age differences beyond error between hydrothermal minerals and igneous minerals (Cathles et al., 1997, Marsh et al., 1997). An exception is the work of Hedenquist, et al. (1998), who studied the young (1.3-1.4 Ma) coupled epithermal-porphyry deposits at Lepanto. Lepanto is an exceptional site for such a study due to its young age and relatively simple thermal history. They were able to discern the difference in age between the coupled advanced argillic-K-silicate alteration (~1.4 Ma) from the later sericite-illite alteration (~1.3 Ma) using K-Ar dating. Additionally, they showed that the peak of the mineralizing event postdated igneous hornblende ages from the host quartz-diorite porphyry by 0.1-0.2 m.y.

There are instances where hydrothermal circulation may last longer. In the case of granites hosting Sn-W mineralization in southwest England, single plutons were sometimes emplaced over 4.5 m.y., and mineralization ages range from synchronous with the host pluton crystallization to up to 40 m.y. later (Chesley et al., 1993). In that case, the series of plutons comprise a batholith emplaced over 25 m.y., and thus likely represents a series of hydrothermal mineralizing events superimposed on one another.

The oldest rock unit dated in this study is the biotite-pyroxenite, here represented by the plateau ages of BMP-7 and RK-3 at 95.9 ± 0.3 Ma and 95.7 ± 0.3 Ma respectively. The diorite body (PB-108) adjacent to the biotite-pyroxenite has an age that overlaps the age of the biotite-pyroxenite within error, though on the young side with a plateau age of 95.3 ± 0.3 Ma. Biotite was dated from the pyroxenite, and hornblende from the diorite, and these minerals have different argon closure temperatures of approximately 500°C and 300°C , respectively (McDougall and Harrison, 1999), at moderate cooling rates. These dated minerals were unaltered primary phases and these ages are interpreted as igneous crystallization/cooling ages. Although within error of the age pyroxenite, these results suggest that the diorite could be slightly younger, due to the difference in closure temperature of the dated minerals.

The earliest evidence for the mineralizing event(s) at Pebble comes from the molybdenite Re-Os age of sample PB-83, which is 89.5 ± 0.3 Ma. This is followed by the hydrothermal biotite from BJT-68 at 88.5 ± 0.3 Ma and the hydrothermal K-feldspar of PB-162 at 86.0 ± 0.2 Ma. The closure temperature of the Re-Os molybdenite geochronometer is essentially magmatic (Stein et al., in press), and it has been known to record crystallization ages through subsequent metasomatic events and even through granulite facies metamorphism (Stein et al., 1998b). The argon closure temperature of biotite is $300\text{-}400^\circ\text{C}$ (McDougall and Harrison, 1999). The argon closure temperature of K-feldspar is variable due to complicated diffusion properties, but is a minimum of 150°C (McDougall and Harrison, 1999).

In a previous study on Pebble, Tracy (2001) used fluid inclusions to constrain homogenization temperatures of quartz veins. He found high salinity inclusions (60-80% NaCl equivalent) to have homogenized at $470\text{-}620^\circ\text{C}$, moderate salinity inclusions (33-55% NaCl equivalent) to have homogenized at $\sim 300\text{-}630^\circ\text{C}$, and low salinity inclusions ($\sim 5\%$ NaCl equivalent) to have homogenized at $300\text{-}500^\circ\text{C}$. Since molybdenite occurs paragenetically late at Pebble, and molybdenite was deposited above the homogenization

temperature of any associated quartz vein, the absolute minimum temperature of molybdenite deposition must be $>300^{\circ}\text{C}$, and is probably substantially higher. At a minimum of 0.4 m.y. after molybdenite deposition, the system was still at least 300°C (biotite BJT-68 age). Assuming a single hydrothermal system, i.e., a system related to one intrusion, this would suggest an implausibly slow cooling rate. At a minimum of 2.0 m.y. after the biotite experienced temperatures of at least 300°C , the K-feldspar experienced minimum temperatures of 150°C . Even disregarding the hydrothermal K-feldspar date, due to its low closure temperature, these data imply a protracted hydrothermal system. These dates are likely not representative of a single, continuous hydrothermal system. Either the dikes and stocks of the porphyry suite were emplaced over several million years, or subsequent thermal events, such as later igneous activity or metamorphism, partially or wholly reset the argon geothermometer.

These findings are in agreement with other combined Re-Os and $^{40}\text{Ar}/^{39}\text{Ar}$ geochronology on ore deposits, such as Watanabe and Stein (2000), where $^{40}\text{Ar}/^{39}\text{Ar}$ geochronology produced younger ages than Re-Os molybdenite geochronology.

The syenite sample PB-79 has an age of 84.1 ± 0.3 Ma, which postdates all dated porphyry alteration by 1.4-2.4 m.y. Other subsurface rocks proximal to the syenite body show evidence of weak porphyry-style alteration (Cominco 1993 unpublished report), however PB-79 shows no evidence of having been altered by externally derived fluids. Specifically, the only alteration sample PB-79 shows is a dusting of sericite on primary K-feldspar; there is no evidence for K-feldspar replacement of plagioclase, the addition of silica, secondary carbonate or recrystallization of primary biotite, and the sample contains no veins. On this basis, the minor alteration is interpreted to be orthomagmatic in nature.

The youngest sample dated in this study is S-91, the vein K-feldspar from the Sill latite, with an integrated (including all of the steps) isochron age of 46.1 ± 0.2 Ma. This age overlaps with the zircon age from the Sill latite of 46.2 ± 0.2 Ma. It should be noted

that the pseudo-plateau age of S-91, at 46.6 ± 0.1 Ma, is older than the zircon from the latite. While it's not impossible that the latite was crystallized over this length of time, it is unlikely, and this lends credence to the use of the whole isochron age as the most correct interpretation.

Geochemistry

Table 3 contains data for rocks collected from drill core and the surface, many of which have been variably altered. It should be noted that the rocks logged as gabbro, listed as Kgb in the lithology code, all contain normative nepheline from 14-23% and normative orthoclase from 27-34%. Although these rocks may have had elevated alkali contents previous to alteration, these numbers suggest significant alteration. The diorite samples (Kd) also contain normative nepheline, although less than the gabbros. It should also be noted that two of the BP samples have SiO₂ contents much lower than the others (38-40 wt. %). These rocks are interpreted to be cumulates, and this is discussed in detail below.

Figures 8 and 9 are Al₂O₃/TiO₂ vs. SiO₂ and Al₂O₃/TiO₂ vs. TiO₂ plots of the lithologies that are found within the Pebble deposit. This includes the porphyry suite (granodiorites of several types and biotite-diorite), diorite and gabbro, but not the granites, latite, syenite or the biotite-pyroxenite. Note that the gabbro and diorite occur both within the alteration zone of the deposit and outside of it, so these samples are included on all diagrams from this data set. These diagrams were chosen to show how ratios and absolute amounts of relatively immobile elements such as Ti and Al differ between lithologies. Figure 8, the Al₂O₃/TiO₂ vs. SiO₂ diagram, and Figure 9, the Al₂O₃/TiO₂ vs. TiO₂ diagram, both show the separate groupings of the various rock types with the exception of the biotitic granodiorite (Kgdb), which plots both with the equigranular diorite and the diorite on Figure 9. Assuming that Al₂O₃ and TiO₂ behave as

Figure 8: $\text{Al}_2\text{O}_3/\text{TiO}_2$ vs. SiO_2 plot for lithologies found within the Pebble deposit. Open triangles = biotite diorite (Kbd), filled triangles = biotitic granodiorite (Kgdb), open squares = equigranular granodiorite (Kgde), filled squares = porphyritic granodiorite (Kgdp), open diamond = porphyritic diorite (Kdp), filled diamonds = gabbro (Kgb), and open circles = diorite (Kd). After Bouley et al. (1995). All oxides are in units of weight %.

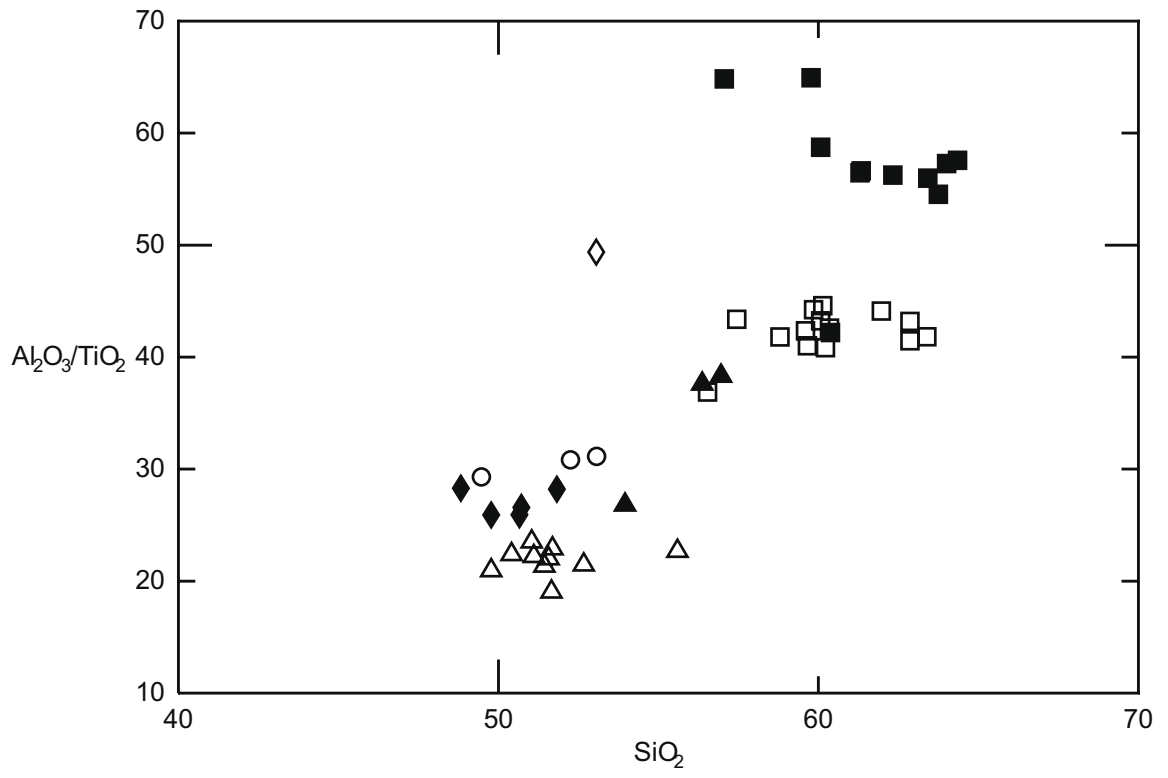
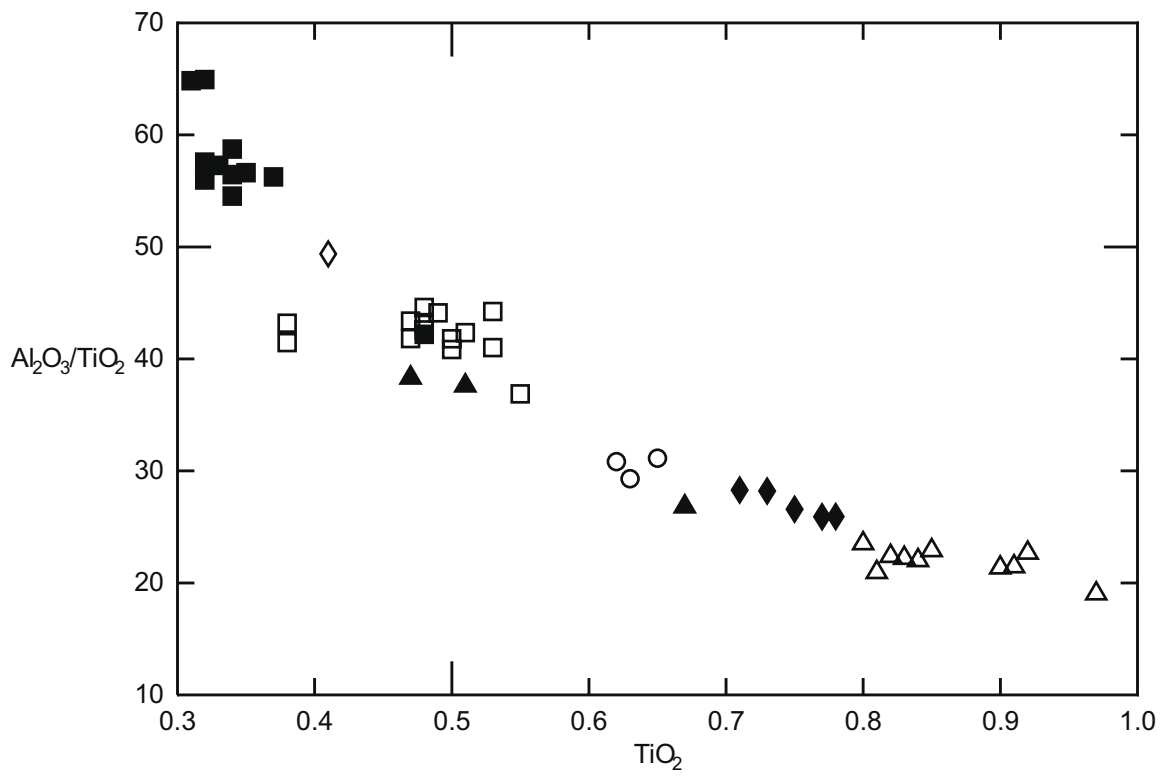


Figure 9: $\text{Al}_2\text{O}_3/\text{TiO}_2$ vs. TiO_2 plot for lithologies found within the Pebble deposit. Symbols are the same as in **Figure 8**. All oxides are in units of weight %.



immobile oxides in the porphyry environment, this discrimination indicates that the different porphyry lithologies, as logged and mapped, are in fact different rocks and not purely textural or alteration facies. The exception is the biotitic granodiorite, which plot with both equigranular granodiorite and between the diorite and gabbro on both diagrams. This may indicate that the biotitic granodiorite, as identified in drill core and mapping, is not a distinct lithology but an alteration facies of both diorites and granodiorites. The porphyry lithologies may be, and likely are, comagmatic, but they represent discrete intrusive events characterized by some differentiation in the parent magma.

Figure 10 is an IUGS SiO_2 -total alkalis nomenclature diagram of the normalized post-mineralization syenites. It includes samples from the Cominco data set (Table 3) and one sample, CS-98-PB78, from this study's data set (Table 4). These rocks are hypabyssal to volcanic, and thus the use of this diagram is justified. One of the samples from this suite plots as a basaltic trachyandesite, one as a trachyandesite and three as trachytes. The only sample observed in thin section would plot as a syenite on the IUGS plutonic diagram, and, if normative analyses were used to classify them, they would plot as syenites and nepheline syenites.

Figure 11 is a collection of Harker diagrams of major oxides plotted against SiO_2 for the syenite/trachyte samples. Generally, the sample points fall onto lines, indicating that they are likely discrete samples from a continuous series of rocks related by fractional crystallization. Furthermore, K_2O , Na_2O and Al_2O_3 correlate positively with SiO_2 content, while MgO , FeO and CaO correlate negatively with SiO_2 , as is expected with evolving magmas. Of these diagrams, the K_2O - SiO_2 and the Na_2O - SiO_2 diagrams show some scatter. Both K_2O and Na_2O are mobile in the presence of fluid, Na_2O being mobile even in ground water, and this likely explains the less than perfect correlations.

Figure 10: $\text{Na}_2\text{O}+\text{K}_2\text{O}$ vs. SiO_2 petrologic diagram for the post-mineralization syenites (Ksy). All oxides are in units of weight %.

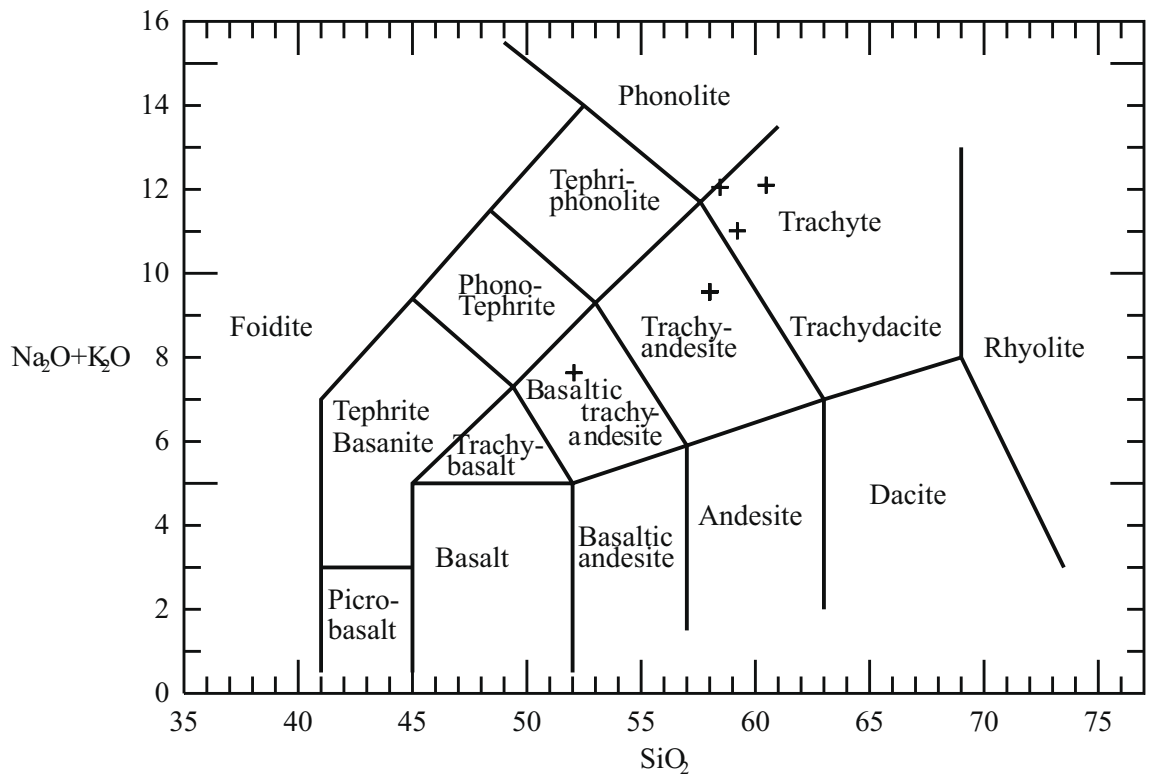
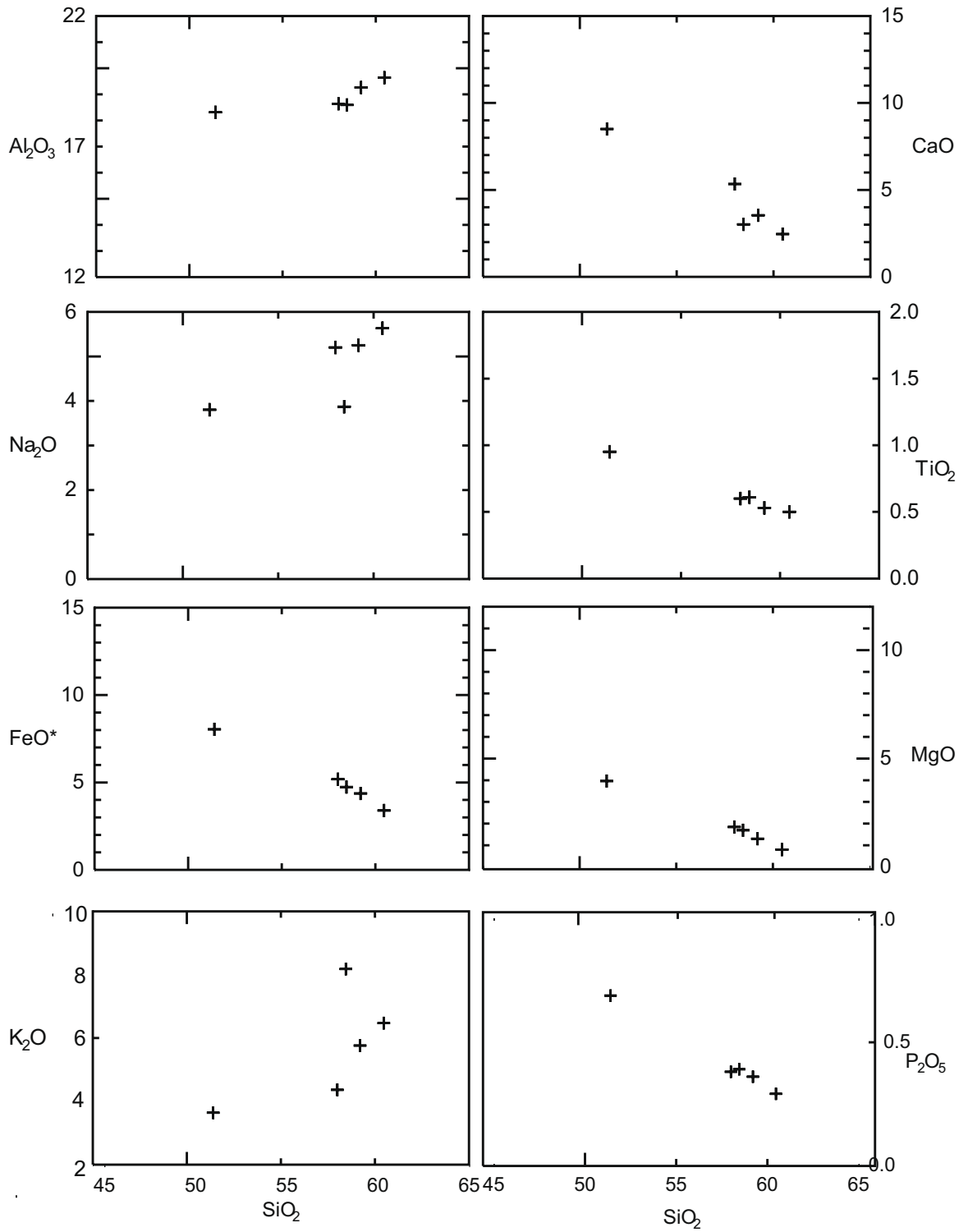


Figure 11: Harker diagrams for the post-mineralization syenites (Ksy). All oxides are in units of weight %.

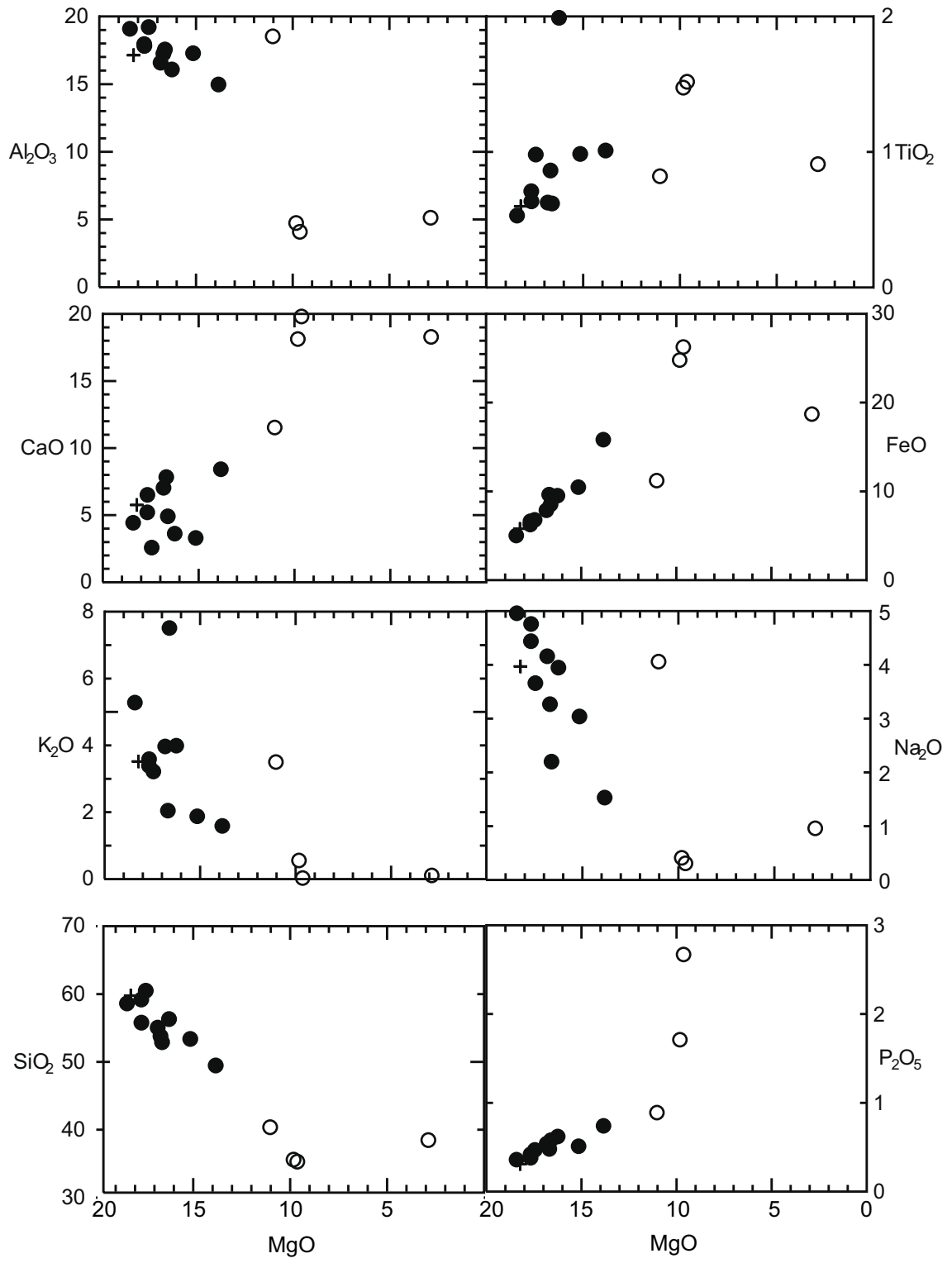


Some of the biotite-pyroxenites show cumulate textures in thin section, with early apatite and clinopyroxene being the dominant cumulate minerals, and magnetite and later apatite as the intercumulate phases (CS98-DBMP1 and CS98-PB141). This is consistent with the very low SiO₂ (35.30 and 35.60 wt%) and high P₂O₅ (2.67 and 1.71 wt%) of these samples. Additionally, CS98-DBMP1 and CS98-PB141 have elevated CaO and MgO relative to the other Kbp samples. These samples do not represent a melt, but minerals separated through fractional crystallization. Two samples from the Cominco data set show anomalously low SiO₂ and high MgO and CaO as well (BP3 and BP4), but with less elevated P₂O₅ (in the case of BP3, the P₂O₅ contents are below the limit of detection). No hand samples or thin sections of BP3 or BP4 were available for examination, but the compositional difference between them and CS98-DBMP1 and CS98-PB141 could be explained by differences in modes of cumulate minerals.

The pre-mineralization biotite-pyroxenites and associated rocks, both from the Cominco data set (Table 3) and from this study's sample set (Table 4), plot as a range of lithologies. The diorite from this study's sample set, PB-108, plots as a monzodiorite on the IUGS plutonic nomenclature chart.. The cumulate samples observed in thin section – PB-141 and D-BMP-1, both plot as clinopyroxenites on the IUGS ultramafic charts, with abundant apatite and magnetite. The dated samples, BMP-7 and RK-3, both contain enough plagioclase (~ 10%) to be classified as gabbros, with abundant biotite. CS98-BMP3 is a biotite pyroxenite, as is CS98-DSY2.

Figure 12 is a set of Fenner diagrams of major oxides plotted against wt % MgO of the biotite-pyroxenites (Kbp). Since they do not represent a melt, plotting the cumulate Kbp samples on Figure 12 is essentially meaningless, but serves to demonstrate how different they are from the noncumulate rocks. Although there is some scatter, SiO₂, Al₂O₃, Na₂O and K₂O inversely correlate with MgO, whereas FeO*, CaO, P₂O₅ and TiO₂ correlate positively with MgO. The trends suggest that noncumulate Kbp samples are part

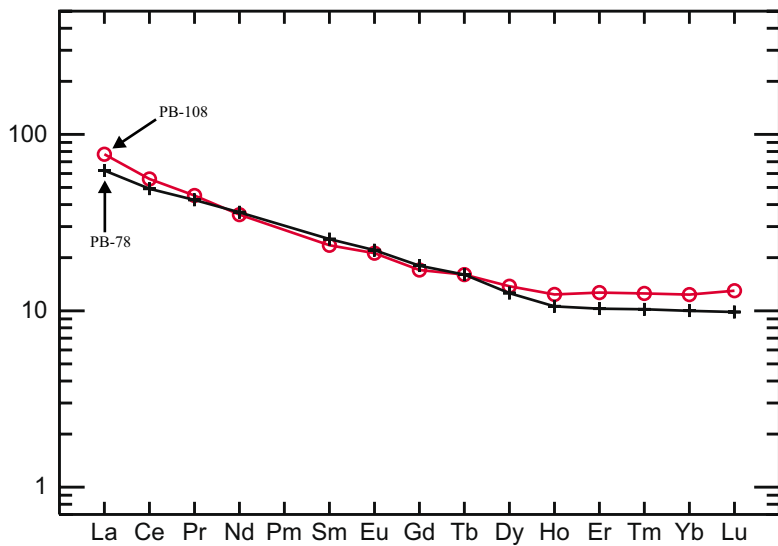
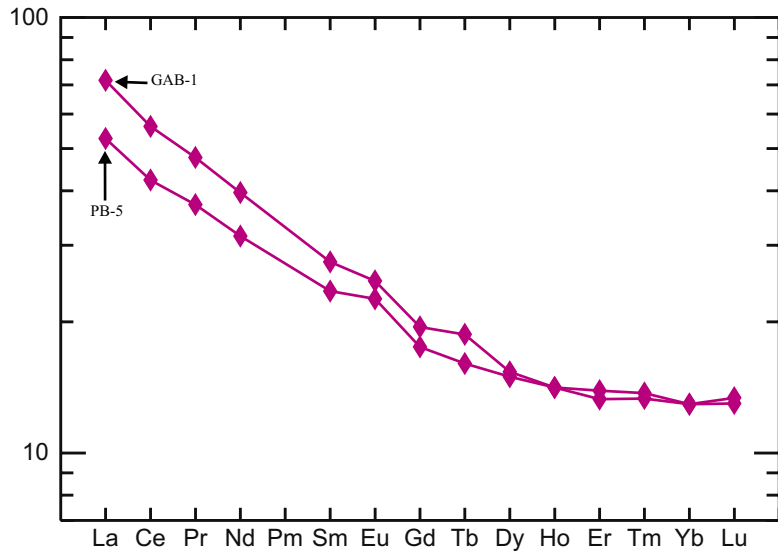
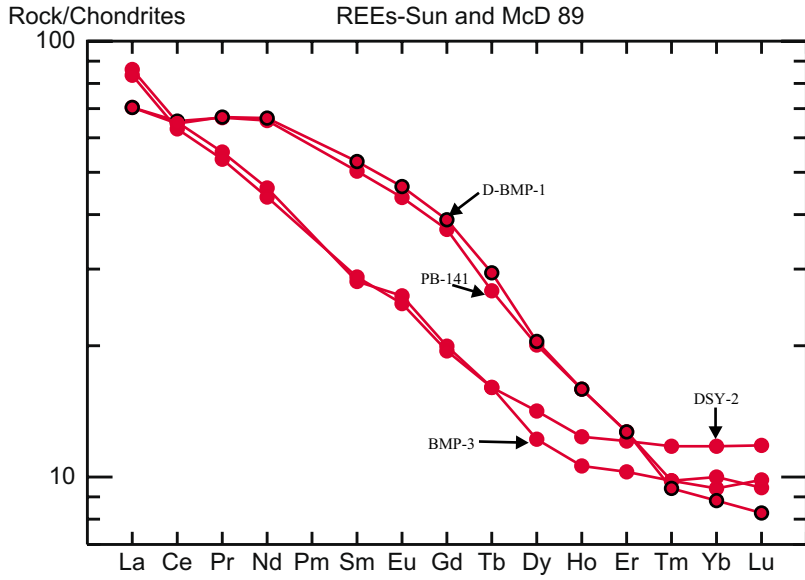
Figure 12: Fenner diagrams for the biotite magnetite series (Kbp) and sample PB-108 (Kd). Filled circles are noncumulate Kbp samples, open circles are cumulate Kbp samples, and the cross is sample PB-108. See text for explanation. All oxides are in units of weight %.



of a magma series related by fractional crystallization, possibly complicated by the presence of xenoliths, as is seen in the thin section of RK-3, or thin cumulate layers. The whole rock composition of the diorite does not differ greatly from that of the biotite pyroxenites, and it generally plots on the same line as compositions of the biotite-pyroxenite series. This, as well as the fact that the dated diorite (PB-108) and dated biotite pyroxenites (BMP-7 and RK-3) are contemporaneous suggests that they are comagmatic. However, only in the SiO_2 and P_2O_5 diagrams does the diorite plot at the end of the series where it would be expected if it were the end product of the same magmatic series. Thus, if the diorite and biotite-pyroxenites are comagmatic, they cannot represent the simplest case of continuous fractional crystallization.

Figure 13 shows chondrite-normalized REE plots of the sample set chosen for this study (Table 4) grouped by lithology. The first diagram contains the patterns for the Kbp samples, cumulates and noncumulates. The noncumulate samples have patterns similar to calc-alkaline or high-K calc-alkaline basalts (Wilson, 1989), with slight positive Eu anomalies. The Eu anomalies may indicate the accumulation of some plagioclase, and may discount an abundance of plagioclase present as restite in the source. However, the Eu anomalies are so small as to be ambiguous. The cumulate samples, DBMP-1 and PB-141, have a pronounced hump in the middle REE. This likely reflects the amount of apatite in these samples. Watson and Green (1981) document the convex upwards pattern of spider diagrams for apatite, as apatite preferentially sequesters middle REE, over a range of compositions and varying activities of H_2O . Additionally, clinopyroxene displays a similar, but less pronounced, convex upwards pattern (Fujimaki, 1986). This has been demonstrated specifically for clinopyroxenes in potassic rocks by Woods and Trigila (2000). The gabbro samples shown in the second diagram have similar patterns to the noncumulate Kbp's, and are probably examples of calc-alkaline to high-K calc-alkaline basaltic magmas crystallizing at depth (Wilson, 1989). Finally, the syenite and diorite in the third diagram also show similar patterns. Most notably, the

Figure 13: Chondrite-normalized rare earth element (REE) spider diagrams. Samples are labeled. See text for explanation.



syenite does not show the enrichment in LREE often present in alkaline rocks (Wilson, 1989).

SECTION 8

CONCLUSIONS

1) The biotite-pyroxenite suite and the diorite predate porphyry mineralization by a minimum of 5.2 m.y., and are not temporally related to ore deposition. Their spatial and temporal proximity to one another and their geochemistry, particularly the trends indicated in the Fenner diagrams, suggest that the biotite-pyroxenite suite and the diorite are comagmatic.

2) Mineralization and alteration events at Pebble can be placed between 89.8 and 85.8 Ma, without any clear bracket on the time of initiation and cessation. The thermal history of the porphyry system can be bracketed by molybdenite crystallization at a minimum of 300°C (and possibly much higher) at 89.5 ± 0.3 Ma and temperatures of $\geq 300^\circ\text{C}$ (biotite closure temperature of sample BJT-68) at 88.5 ± 0.3 Ma. Less reliably, the K-feldspar sample experienced temperatures of $\geq 150^\circ\text{C}$ at 86.0 ± 0.2 Ma. This is too long for a hydrothermal system fueled by a single intrusion or contemporaneous intrusions. This indicates a more protracted thermal history than most geochronologic studies on porphyry systems indicate.

3) The syenite cooled to $\geq 300^\circ\text{C}$ at least 1.4 m.y. after the last known porphyry-related alteration, and is likely a post ore deposition.

4) Epithermal mineralization at Sill is essentially synchronous with crystallization of its latite host rock, and is related to Tertiary magmatism. The mineralization postdates Cretaceous porphyry mineralization by ~ 35 m.y.

5) The Pebble claim block contains more alkalic rocks than do typical continental arc assemblages (i.e., biotite magnetite pyroxenite, nepheline-normative diorites, syenite and latite). Despite the prevalence of alkalic rocks before and after the porphyry mineralization, the relict plagioclase and quartz phenocrysts in the granodiorite suite

indicate that they are nonalkaline igneous rocks. However, More work should be done to better constrain the pre-alteration composition of the porphyry suite to aid in exploration target identification.

REFERENCES

- Beane, R.E., and Titley, S.R., 1981, Porphyry copper deposits, Part II: Hydrothermal alteration and mineralization, in Economic Geology Seventy-fifth Anniversary Volume, ed. by Brian J. Skinner, Lancaster Press, Lancaster, Pennsylvania, pp. 235-269.
- Bouley, B.A., St. George, P., and Wetherbee, P.K, 1995, Geology and discovery at Pebble Copper, a copper-gold porphyry system in southwest Alaska, Canadian Institute of Mining, Metallurgy and Petroleum Special Volume 46, p.422-435.
- Cathles, L.M., Erendi, A.H.J., and Barrie, T., 1997, How long can a hydrothermal system be sustained by a single intrusive event?, *Economic Geology*, v. 92, p. 766-771.
- Chesley, J.T., Halliday, A.N., Snee, L.W., Mezger, K., Shepherd, T.J., and Scrivener, R.C., 1993, Thermochronology of the Cornubian batholith: Implications for pluton emplacement and protracted hydrothermal mineralization, *Geochimica et Cosmochimica Acta*, v. 57, p. 1817-1837.
- Dalrymple, G.B., and Lanphere, M.A., 1974, $^{40}\text{Ar}/^{39}\text{Ar}$ age spectra of some undisturbed terrestrial samples, *Geochimica et Cosmochimica Acta*, v. 38, p. 715-738.
- Deer, W.A., Howie, R.A., Zussman, J., 1966, An Introduction to the Rock Forming Minerals, Longman, Great Britain, 528 p.

- Detterman, R.L., and Reed, B.L., 1980, Stratigraphy, structure, and economic geology of the Iliamna quadrangle, *Alaska, U.S. Geological Survey Bulletin 1368-B*, 86 p., scale 1:250,000.
- Foland, K.A., Gilbert, L.A., Sebring, C.A., and Chen, J.F., 1986, $^{40}\text{Ar}/^{39}\text{Ar}$ ages for plutons of the Montereian Hills, Quebec; Evidence for a single episode of Cretaceous magmatism, *Geological Society American Bulletin*, v. 97, p.966-974.
- Fujimaki, Hirokazu, 1986, Partition coefficients of Hf, Zr, and REE between zircon, apatite and liquid, *Contributions to Mineralogy and Petrology*, v. 94, p. 42-45.
- Goldfarb, R.J., 1997, Metallogenic evolution of Alaska, Economic Geology Monograph 9, p. 4-34.
- Hedenquist, J.W., Arribas, A., Jr., and Reynolds, T.J., 1998, Evolution of an intrusion-centered hydrothermal system: Far Southeast Lepanto porphyry and epithermal Su-Au deposits, Philippines, *Economic Geology*, v.93, p. 373-404.
- Henderson, P., 1984, General geochemical properties and abundances of the rare earth elements, in Rare Earth Element Geochemistry, ed. by P. Henderson, Elsevier, Amsterdam, p. 1-32.
- Lanphere, M.A., and Dalrymple, G.B., 1978, The use of $^{40}\text{Ar}/^{39}\text{Ar}$ data in evaluation of disturbed K-Ar systems, *U.S. Geological Survey Open-file Report 78-701*, p. 241-243.

- Layer, P.W., Hall, C.M., and York, D., 1987, The derivation of $^{40}\text{Ar}/^{39}\text{Ar}$ age spectra of single grains of hornblende and biotite by laser step-heating, *Geophysical Research Letters*, v. 14, p. 757-760.
- Keith, J.D., Whitney, J.A., Hattori, K., Ballantyne, G.H., Christiansen, E.H., Barr, D.L., Cannan, T.M., and Hook, C.J., 1997, The role of magmatic sulfides and mafic alkaline magmas in the Bingham and Tintic mining districts, Utah, *Journal of Petrology*, v. 38, p.1679-1690.
- Marsh, Timothy M., Einaudi, Marco T., and McWilliams, Michael, 1997, $^{40}\text{Ar}/^{39}\text{Ar}$ geochronology of Cu-Au and Au-Ag mineralization in the Potrerillos district, Chile, *Economic Geology*, v. 92, 784-806.
- McDougall, I. and Harrison, T.M., 1999, Geochronology and Thermochronology by the $^{40}\text{Ar}/^{39}\text{Ar}$ Method-2nd ed, Oxford University Press, New York, 269pp.
- Muller, Daniel, and Groves, David I., 1995, Potassic Igneous Rocks and Associated Gold-Copper Mineralization, Springer, Berlin, 210 pp.
- Norton, D., and Knight, J., 1977, Transport phenomena in hydrothermal ore systems: Cooling plutons, *American Journal of Science*, v. 277, p. 937-981.
- Smoliar, Michael I., Walker, Richard J., Morgan, John W., 1996, Re-Os ages for group IIA, IIIA, IVA, and IVB iron meteorites, *Science*, v. 271: 5252, p. 1099-1102.
- Stein, H.J., Markey, R.J., Morgan, J.W., Hannah, J.L., and Schersten, A., The remarkable Re-Os chronometer: how and why it works, (in press), *Terra Nova*.

- Stein, H.J., Morgan, J.W., Markey, R.J., and Hannah, J.L. (1998a) An introduction to Re-Os: What's in it for the mineral industry?: *SEG Newsletter*, v. 32, p. 1, 8-15.
- Stein, H.J., Sundblad, K., Markey, R.J., Morgan, J.W., and Motuza, G. (1998b) Re-Os ages for Archean molybdenite and pyrite, Kuittila-Kivisuo, Finland and Proterozoic molybdenite, Kabeliai, Lithuania: testing the chronometer in a metamorphic and metasomatic setting: *Mineralium Deposita*, v. 33, p. 329-345.
- Sun, S.S., and McDonough, W.F., 1989, Chemical and isotopic systematics of oceanic basalts: implications for mantle compositions and processes, in Saunders, A.D. and Norry, M.J., Magmatism in the Ocean Basins, Geol. Soc. Spec. Pub. No. 42, p. 313-345.
- Tracy, B.J., 2001, Geology and fluid geochemistry of the Pebble Cu-Au porphyry deposit, southwest Alaska, unpublished M.S. thesis, University of Georgia, 148 p
- Villa, I. M., 1998, Isotopic Closure, *Terra Nova*, v. 10, p. 42-47.
- Watanabe, Yasushi and Stein, Holly J., 2001, Re-Os ages for the Erdenet and Tsagaan Suvarga porphyry Cu-Mo deposits, Mongolia, and tectonic implications, *Economic Geology*, 95:7, p.1537-1542.
- Watson, E. Bruce, and Green, Trevor H., 1981, Apatite/liquid partition coefficients for the rare earth elements and strontium, *Earth and Planetary Science Letters*, v. 56, p. 405-421.

- White, D.E., and Heropolous, C., 1986, Active and fossil hydrothermal convective systems of the Great Basin, *Geothermal Research Council Special Report*, p. 41-53.
- Wilson, Marjorie, 1989, *Igneous Petrogenesis*, Unwin hyman, London. 466 pp.
- Wood, Bernard J., and Trigila, Raffaello, 2001, Experimental determination of aluminous clinopyroxene-melt partition coefficients for potassic liquids, with application to the evolution of the Roman province potassic magmas, *Chemical Geology*, v. 172, p. 213-223.
- Young, L.E., St. George, P., and Bouley, B.A., 1997, Porphyry copper deposits in relation to the magmatic history and palinspastic restoration of Alaska, *Economic Geology Monograph 9*, p.306-333.
- York, D., Hall, C.M., Yanase, Y., Hanes, J.A., and Kenyon, W.J., 1981, $^{40}\text{Ar}/^{39}\text{Ar}$ dating of terrestrial minerals with a continuous laser, *Geophysical Research Letters*, v. 8, p. 1136-1138.

APPENDIX A

ELECTRON MICROPROBE ANALYSIS RESULTS.

Electron microprobe analyses for clinopyroxenes from Kbp suite									
sample	BMP-3	BMP-3	BMP-3	BMP-3	BMP-3	BMP-3	BMP-3	RK-3	
analysis	cpx-x1	cpx-x2	cpx-x3	cpx-1	cpx-2	cpx-2	cpx-2	cpx-x1	
notes	xenolith	xenolith	xenolith					xenolith	
<i>weight %</i>									
SiO2	49.00	49.24	49.43	51.33	51.51	51.51	51.51	50.56	
Al2O3	4.04	3.94	3.83	2.12	2.29	2.29	2.29	3.52	
TiO2	0.70	0.66	0.64	0.42	0.37	0.37	0.37	0.56	
CaO	23.10	24.21	23.08	23.22	22.87	22.87	22.87	23.16	
MgO	13.48	13.68	13.74	14.33	14.06	14.06	14.06	14.29	
FeO(t)	7.60	7.19	7.10	6.89	7.71	7.71	7.71	6.72	
MnO	0.20	0.25	0.25	0.49	0.45	0.45	0.45	0.29	
Cr2O3	-	-	0.01	-	-	-	-	-	
K2O	-	-	0.01	0.03	-	-	-	-	
Na2O	0.43	0.43	0.43	0.53	0.68	0.68	0.68	0.38	
Total	98.55	99.60	98.52	99.36	99.94	99.94	99.94	99.48	
<i>number of ions on the basis of 6 O's, tetrahedral site set to 2.000</i>									
Si	1.861	1.853	1.873	1.925	1.925	1.925	1.925	1.890	
T Al	0.139	0.147	0.127	0.075	0.075	0.075	0.075	0.110	
Al (total)	0.181	0.175	0.171	0.094	0.101	0.101	0.101	0.155	
M Al	0.042	0.028	0.043	0.019	0.026	0.026	0.026	0.045	
Ti	0.020	0.019	0.018	0.012	0.010	0.010	0.010	0.016	
Ca	0.940	0.976	0.937	0.933	0.916	0.916	0.916	0.927	
Mg	0.763	0.768	0.776	0.801	0.783	0.783	0.783	0.796	
Fe2	0.241	0.226	0.225	0.216	0.241	0.241	0.241	0.210	
Mn	0.006	0.008	0.008	0.016	0.014	0.014	0.014	0.009	
Cr	-	-	-	-	-	-	-	-	
K	-	-	-	0.001	-	-	-	-	
Na	0.032	0.031	0.032	0.039	0.049	0.049	0.049	0.028	
<i>normalized molecular % cations</i>									
Ca%	48.18	49.35	48.14	47.46	46.86	46.86	46.86	47.73	
Mg%	39.12	38.81	39.88	40.76	40.09	40.09	40.09	40.98	
Fe%	12.37	11.44	11.56	10.99	12.33	12.33	12.33	10.81	
Mn%	0.33	0.40	0.41	0.79	0.73	0.73	0.73	0.47	
dashes (-) indicate values below the detection limit									

Electron microprobe analyses for clinopyroxenes from Kbp suite												
sample	RK-3		PB-121		PB-121		PB-121		D-BMP-1	D-BMP-1		
analysis	cpx-x2		cpx-1		cpx-2		cpx-3		cpx-1	cpx-2		
notes	xenolith								cumulate	cumulate		
<i>weight %</i>												
SiO2	49.98		48.23		48.86		48.86		49.78	48.51		
Al2O3	3.64		4.91		4.46		4.20		3.35	4.66		
TiO2	0.56		0.91		0.83		0.82		0.59	0.84		
CaO	22.95		23.30		24.17		23.62		24.17	23.46		
MgO	13.65		13.04		13.33		13.64		14.20	13.21		
FeO(t)	6.83		7.71		7.69		6.97		6.80	7.40		
MnO	0.26		0.20		0.26		0.18		0.20	0.25		
Cr2O3	-		-		0.04		-		-	-		
K2O	-		0.03		0.02		-		-	-		
Na2O	0.45		0.52		0.43		0.43		0.37	0.29		
Total	98.32		98.85		100.09		98.72		99.46	98.62		
<i>number of ions on the basis of 6 O's, tetrahedral site set to 2.000</i>												
Si	1.891	} 2.000	1.831	} 2.000	1.835	} 2.000	1.851	} 2.000	1.871	} 2.000	1.842	} 2.000
T Al	0.109		0.169		0.165		0.149		0.129		0.158	
Al (total)	0.162		0.220		0.197		0.187		0.148		0.209	
M Al	0.054	} 2.028	0.051	} 2.053	0.033	} 2.058	0.038	} 2.048	0.019	} 2.052	0.050	} 2.041
Ti	0.016		0.026		0.023		0.023		0.017		0.024	
Ca	0.930		0.948		0.973		0.958		0.973		0.954	
Mg	0.770		0.738		0.746		0.770		0.796		0.748	
Fe2	0.216		0.245		0.242		0.221		0.214		0.235	
Mn	0.008		0.006		0.008		0.006		0.006		0.008	
Cr	-		-		0.001		-		-		-	
K	-		0.001		0.001		-		-		-	
Na	0.033	0.038	0.031	0.032	0.027	0.021						
<i>normalized molecular % cations</i>												
Ca%	48.33		48.93		49.40		49.02		48.93	49.06		
Mg%	40.00		38.10		37.91		39.39		40.00	38.44		
Fe%	11.23		12.64		12.27		11.29		10.74	12.08		
Mn%	0.43		0.33		0.42		0.30		0.32	0.41		
dashes (-) indicate values below the detection limit												

Electron microprobe analyses for clinopyroxenes from Kbp suite											
sample	D-BMP-1		D-BMP-1		D-BMP-1						
analysis	cpx-3		cpx-4		cpx-5						
notes	cumulate		cumulate		cumulate						
<i>weight %</i>											
SiO2	49.26		49.06		48.73						
Al2O3	3.92		4.37		4.63						
TiO2	0.71		0.80		0.82						
CaO	24.42		23.60		24.52						
MgO	13.76		13.57		13.56						
FeO(t)	6.89		7.16		7.47						
MnO	0.18		0.15		0.23						
Cr2O3	-		-		-						
K2O	-		-		-						
Na2O	0.29		0.40		0.35						
Total	99.43		99.11		100.31						
<i>number of ions on the basis of 6 O's, tetrahedral site set to 2.000</i>											
Si	1.854	} 2.000	1.851	} 2.000	1.826	} 2.000					
T Al	0.146		0.149		0.174						
Al (total)	0.174		0.194		0.204						
M Al	0.028	} 2.049	0.045	} 2.044	0.030	} 2.062					
Ti	0.020		0.023		0.023						
Ca	0.985		0.954		0.984						
Mg	0.772		0.763		0.757						
Fe2	0.217		0.226		0.234						
Mn	0.006		0.005		0.007						
Cr	-		-		-						
K	-		-		-						
Na	0.021	0.029	0.025								
<i>normalized molecular % cations</i>											
Ca%	49.75		48.97		49.63						
Mg%	39.01		39.19		38.20						
Fe%	10.96		11.60		11.80						
Mn%	0.29		0.25		0.37						
<i>dashes (-) indicate values below the detection limit</i>											

Electron microprobe analyses for biotite from Kbp suite												
sample	BMP-3		BMP-3		BMP-3		BMP-7		BMP-7		BMP-7	
analysis	bt-x1		bt-1		bt-2		bt-1		bt-2		bt-3	
notes	xenolith											
<i>weight %</i>												
SiO2	38.80		37.60		37.36		35.71		36.62		35.56	
Al2O3	14.31		13.41		13.79		14.84		16.22		15.30	
TiO2	6.01		5.63		5.58		4.33		4.52		3.96	
MgO	18.27		13.74		16.41		16.32		15.51		14.94	
FeO(t)	9.96		16.42		11.38		12.44		13.65		14.32	
MnO	0.18		0.37		0.26		0.23		0.25		0.16	
CaO	0.05		0.07		0.05		0.10		0.22		-	
K2O	9.61		10.26		9.66		9.60		9.31		9.28	
Na2O	0.26		0.10		0.23		0.40		0.33		0.25	
BaO	0.09		0.05		0.10		0.29		0.15		0.09	
F	0.54		0.78		0.81		1.01		0.17		0.49	
Cl	0.12		0.10		0.13		0.10		0.07		0.05	
Total'	98.20		98.53		95.76		95.37		97.02		94.40	
-O=F	0.23		0.328		0.34		0.43		0.07		0.21	
-O=Cl	0.03		0.023		0.03		0.02		0.02		0.01	
Total	97.95		98.18		95.39		94.92		96.93		94.18	
<i>number of ions on the basis of 24 (O, OH, F, Cl)'s, tetrahedral site set to 8.000, OH,F,Cl site set to 4.00</i>												
Si	6.005	} 8.000	6.018	} 8.000	5.995	} 8.000	5.810	} 8.000	5.846	} 8.000	5.865	} 8.000
T Al	1.995		1.982		2.005		2.190		2.154		2.135	
Al (total)	2.610		2.529		2.608		2.846		3.052		2.974	
M Al	0.615	} 6.842	0.547	} 6.751	0.603	} 6.765	0.656	} 6.868	0.897	} 6.987	0.839	} 7.000
Ti	0.700		0.678		0.673		0.530		0.543		0.491	
Mg	4.215		3.278		3.926		3.959		3.691		3.673	
Fe2	1.289		2.197		1.527		1.692		1.822		1.975	
Mn	0.024		0.050		0.035		0.032		0.034		0.022	
Ca	0.008		0.012		0.009		0.017		0.038		-	
K	1.897	} 1.989	2.095	} 2.141	1.977	} 2.064	1.992	} 2.155	1.896	} 2.045	1.952	} 2.038
Na	0.078		0.031		0.072		0.126		0.102		0.080	
Ba	0.005		0.003		0.006		0.018		0.009		0.006	
F	0.264	} 4.000	0.395	} 4.000	0.411	} 4.000	0.520	} 4.000	0.086	} 4.000	0.256	} 4.000
Cl	0.031		0.027		0.035		0.028		0.019		0.014	
OH (ideal)	3.704		3.578		3.554		3.453		3.895		3.730	
<i>normalized molecular % cations</i>												
Fe%	53.24		40.13		28.0		29.95		33.05		34.96	
Mg%	46.76		59.87		72.0		70.05		66.95		65.04	
dashes (-) indicate values below the detection limit												

Electron microprobe analyses for biotite from Kbp suite												
sample	PB-121		PB-121		PB-121		PB-139		PB-139			
analysis	bt-1		bt-2		bt-3		bt-1		bt-2			
notes												
<i>weight %</i>												
SiO ₂	37.17		37.35		37.42		37.90		36.96		38.24	
Al ₂ O ₃	16.40		16.26		16.06		16.73		16.04		16.42	
TiO ₂	3.65		3.88		4.68		4.01		3.79		3.64	
MgO	18.25		18.41		18.91		18.20		17.88		18.23	
FeO(t)	10.29		10.46		9.04		10.32		10.21		10.95	
MnO	0.13		0.14		0.15		0.12		0.11		0.10	
CaO	0.09		0.02		0.03		n.d.		n.d.		n.d.	
K ₂ O	10.11		8.24		10.30		5.49		7.71		5.26	
Na ₂ O	0.46		0.45		0.53		0.31		0.46		0.39	
BaO	0.32		0.27		0.25		0.35		0.35		0.33	
F	0.23		0.29		0.30		0.21		0.33		0.35	
Cl	0.09		0.05		0.04		0.05		0.05		0.05	
Total'	97.19		95.82		97.71		93.69		93.89		93.96	
-O=F	0.10		0.122		0.13		0.09		0.14		0.15	
-O=Cl	0.02		0.011		0.01		0.01		0.01		0.01	
Total	97.07		95.69		97.57		93.59		93.74		93.80	
<i>number of ions on the basis of 24 (O, OH, F, Cl)'s, tetrahedral site set to 8.000, OH,F,Cl site set to 4.00</i>												
Si	5.857	} 8.000	5.901	} 8.000	5.837	} 8.000	6.001	} 8.000	5.940	} 8.000	6.044	} 8.000
T Al	2.143		2.099		2.163		1.999		2.060		1.956	
Al (total)	3.046		3.027		2.952		3.122		3.038		3.058	
M Al	0.903	} 6.996	0.928	} 7.126	0.789	} 6.934	1.122	} 7.278	0.978	} 7.108	1.102	} 7.290
Ti	0.433		0.461		0.549		0.478		0.458		0.433	
Mg	4.287		4.336		4.397		4.296		4.284		4.295	
Fe ₂	1.356		1.382		1.179		1.366		1.372		1.447	
Mn	0.017		0.019		0.020		0.016		0.015		0.013	
Ca	0.015	0.003	0.005	n.d.	n.d.	n.d.						
K	2.032	} 2.208	1.661	} 1.819	2.049	} 2.230	1.109	} 1.226	1.581	} 1.746	1.060	} 1.200
Na	0.141		0.138		0.160		0.095		0.143		0.119	
Ba	0.020		0.017		0.015		0.022		0.022		0.020	
F	0.115	} 4.000	0.145	} 4.000	0.148	} 4.000	0.105	} 4.000	0.168	} 4.000	0.175	} 4.000
Cl	0.024		0.013		0.011		0.013		0.014		0.013	
OH (ideal)	3.861		3.842		3.841		3.881		3.819		3.812	
<i>normalized molecular % cations</i>												
Fe%	24.03		24.17		21.1		24.13		24.26		25.20	
Mg%	75.97		75.83		78.9		75.87		75.74		74.80	
<i>dashes (-) indicate values below the detection limit, n.d. = not determined</i>												

Electron microprobe analyses for biotite from Kbp suite											
sample	PB-139										
analysis	bt-4										
notes											
	<i>weight %</i>										
SiO2	36.95										
Al2O3	16.29										
TiO2	3.68										
MgO	18.39										
FeO(t)	9.88										
MnO	0.11										
CaO	n.d.										
K2O	9.45										
Na2O	0.57										
BaO	0.41										
F	0.19										
Cl	0.08										
Total'	96.00										
-O=F	0.08										
-O=Cl	0.02										
Total	95.90										
<i>number of ions on the basis of 24 (O, OH, F, Cl)'s, tetrahedral site set to 8.000, OH,F,Cl site set to 4.00</i>											
Si	5.869	}	8.000								
T Al	2.131										
Al (total)	3.049										
M Al	0.918	}	7.038								
Ti	0.440										
Mg	4.354										
Fe2	1.312										
Mn	0.015										
Ca	n.d.										
K	1.914	}	2.116								
Na	0.176										
Ba	0.026										
F	0.095	}	4.000								
Cl	0.022										
OH (ideal)	3.883										
<i>normalized molecular % cations</i>											
Fe%	23.16										
Mg%	76.84										
<i>dashes (-) indicate values below the detection limit, n.d. = not determined</i>											

Electron microprobe analyses for hornblende						
sample	PB-108		PB-108			
analysis	amph-1		amph-2			
<i>weight %</i>						
SiO2	42.15		42.37			
Al2O3	10.74		12.32			
TiO2	2.19		1.83			
MgO	10.27		11.34			
FeO(t)	17.39		14.48			
Cr2O3	0.02		0.13			
MnO	0.53		0.32			
CaO	11.81		11.40			
K2O	1.67		0.93			
Na2O	1.83		2.02			
BaO	0.05		0.00			
F	0.27		0.31			
Cl	0.12		0.03			
Total'	99.04		97.48			
-O=F	0.11		0.131			
-O=Cl	0.03		0.007			
Total	98.90		97.34			
<i>number of ions on the basis of 24 (O, OH, F, Cl)'s, tetrahedral site set to 8.000, OH,F,Cl site set to 2.00</i>						
Si	6.614	} 8.000	6.604	} 8.000		
T Al	1.386		1.396			
Al (total)	1.986		2.263			
M Al	0.600	} 5.616	0.866	} 5.661		
Ti	0.258		0.215			
Mg	2.403		2.635			
Fe2	2.282		1.887			
Cr2	0.002		0.016			
Mn	0.070		0.042			
Ca	1.985		1.903			
K	0.334	} 2.879	0.185	} 2.699		
Na	0.557		0.610			
Ba	0.003		0.000			
F	0.134	} 2.000	0.153	} 2.000		
Cl	0.032		0.008			
OH (ideal)	1.834		1.839			

APPENDIX B

DATA TABLES FOR $^{40}\text{Ar}/^{39}\text{Ar}$ STEP HEATING ANALYSES.

078-07 BMP-7 BI 07-27-99 PEBBLE

Weighted average of J from standards = 0.008658 +/- 0.000022

Laser Power (mW)	Cumulative 39Ar	40Ar/39Ar measured	+/-	37Ar/39Ar measured	+/-	36Ar/39Ar measured	+/-	% Atmospheric 40Ar	Ca/K	+/-	Cl/K	+/-	40*/39K	+/-	Age (Ma)	+/- (Ma)
150	0.0006	1289.937	18.37811	-0.14349	0.05191	4.30704	0.06562	98.66906	-0.26325	0.09522	0.00788	0.00626	17.16633	6.91686	249.98	94.06
300	0.0028	159.4307	1.6593	0.01653	0.02125	0.52495	0.00795	97.31424	0.03032	0.03899	0.00665	0.00092	4.2812	1.72331	65.66	25.96
600	0.0454	19.26284	0.04629	0.00287	0.00062	0.04271	0.00053	65.62089	0.00527	0.00114	0.00855	0.0001	6.61254	0.15588	100.44	2.3
750	0.1296	10.80323	0.01299	0.00209	0.00036	0.01495	0.00006	40.98862	0.00384	0.00066	0.00851	0.00009	6.35821	0.02052	96.67	0.3
900	0.2307	7.81627	0.02047	0.00789	0.00026	0.00512	0.00011	19.42573	0.01447	0.00048	0.00797	0.00008	6.27481	0.03598	95.44	0.53
1050	0.33	6.76882	0.01147	0.0162	0.00049	0.00128	0.00006	5.59087	0.02972	0.0009	0.00804	0.00012	6.36336	0.02167	96.75	0.32
1250	0.4269	6.71336	0.01176	0.03051	0.00066	0.00127	0.00006	5.58502	0.05598	0.00122	0.00804	0.00008	6.31145	0.02093	95.98	0.31
1500	0.5465	6.59623	0.01264	0.02545	0.00058	0.00088	0.00005	3.9242	0.04671	0.00107	0.0081	0.00011	6.30991	0.0203	95.96	0.3
1750	0.6791	6.51236	0.00926	0.02726	0.00031	0.00064	0.0001	2.87272	0.05002	0.00057	0.00798	0.00007	6.29751	0.03153	95.78	0.47
2000	0.7741	6.53202	0.00986	0.01938	0.00048	0.00075	0.00008	3.39603	0.03556	0.00089	0.00814	0.00007	6.28255	0.02517	95.55	0.37
2250	0.8085	6.82571	0.01777	0.00779	0.00076	0.00151	0.00021	6.55731	0.01429	0.0014	0.00797	0.00012	6.35134	0.06543	96.57	0.97
2500	0.8347	6.55389	0.0166	0.00476	0.00132	0.00085	0.00026	3.83768	0.00873	0.00242	0.00815	0.00016	6.2748	0.07962	95.44	1.18
2750	0.8535	6.66455	0.01807	0.0027	0.00123	0.00089	0.00034	3.95429	0.00495	0.00226	0.00796	0.00021	6.37346	0.10237	96.9	1.52
3000	0.9172	6.5105	0.01545	0.00857	0.00064	0.00051	0.0001	2.33458	0.01572	0.00118	0.00828	0.00007	6.33051	0.03295	96.26	0.49
3500	0.9377	6.7082	0.01913	0.00115	0.00138	0.00134	0.00029	5.93191	0.00211	0.00253	0.00865	0.00014	6.28328	0.08713	95.56	1.29
8500	1	6.6594	0.01828	0.00106	0.00042	0.00121	0.00014	5.4005	0.00195	0.00077	0.00872	0.00012	6.27261	0.04398	95.41	0.65
Integrated		8.79769	0.00497	0.01518	0.00016	0.00827	0.00004	27.84559	0.02786	0.0003	0.00817	0.00003	6.32728	0.01267	96.22	0.31

UAF078-09 RK-3 BI 07-26-99 PEBBLE

Weighted average of J from standards = 0.008658 +/- 0.000022

Laser Power (mW)	Cumulative 39Ar	40Ar/39Ar measured	+/-	37Ar/39Ar measured	+/-	36Ar/39Ar measured	+/-	% Atmospheric 40Ar	Ca/K	+/-	Cl/K	+/-	40*/39K	+/-	Age (Ma)	+/- (Ma)
150	0.001	106.8545	1.4513	0.13543	0.0197	0.34644	0.00843	95.82281	0.24851	0.03615	0.11035	0.00239	4.4627	2.08289	68.39	31.32
200	0.0022	29.66101	0.30303	0.16096	0.01851	0.09413	0.00548	93.83006	0.29536	0.03396	0.03324	0.002	1.82849	1.59723	28.34	24.56
300	0.0067	15.74957	0.15849	0.22305	0.00727	0.03319	0.00194	62.28321	0.40933	0.01335	0.02253	0.00079	5.93027	0.56859	90.33	8.45
450	0.0258	9.14315	0.03586	0.09342	0.00297	0.01059	0.00044	34.25655	0.17143	0.00545	0.01892	0.00012	5.99252	0.1313	91.25	1.95
600	0.0632	7.78468	0.01649	0.05975	0.00105	0.0053	0.00021	20.13106	0.10964	0.00193	0.01819	0.00019	6.19486	0.06333	94.25	0.94
750	0.1122	7.21696	0.02247	0.06198	0.0009	0.0033	0.00012	13.50079	0.11373	0.00164	0.01759	0.00015	6.21804	0.03955	94.6	0.59
900	0.1689	7.0291	0.0194	0.04986	0.00071	0.00245	0.0001	10.29031	0.09148	0.00131	0.01764	0.00015	6.28024	0.03547	95.52	0.53
1050	0.2219	6.89806	0.01802	0.06841	0.00102	0.00223	0.00008	9.53383	0.12552	0.00187	0.01752	0.0002	6.21473	0.02975	94.55	0.44
1250	0.2888	6.96129	0.01152	0.07726	0.00062	0.00236	0.00006	9.96365	0.14177	0.00114	0.01836	0.00012	6.24217	0.02122	94.96	0.31
1500	0.3785	6.80797	0.01003	0.07496	0.00071	0.00176	0.00009	7.57082	0.13755	0.0013	0.01828	0.00009	6.26633	0.02856	95.31	0.42
2000	0.5757	6.6467	0.01779	0.08114	0.00019	0.00149	0.00003	6.54433	0.14889	0.00035	0.01859	0.00005	6.18523	0.02017	94.11	0.3
3000	0.8508	6.55791	0.02186	0.09542	0.00032	0.00122	0.00002	5.41532	0.1751	0.00059	0.0193	0.00006	6.17602	0.02264	93.97	0.34
4000	0.9737	6.49291	0.00503	0.071	0.00084	0.00064	0.00006	2.84439	0.13027	0.00154	0.0176	0.00008	6.28064	0.01731	95.53	0.26
8500	1	6.56268	0.02137	0.08129	0.00149	0.00098	0.00023	4.31985	0.14915	0.00273	0.01733	0.00027	6.25205	0.06977	95.1	1.03
Integrated		6.95738	0.0074	0.07985	0.0002	0.00247	0.00002	10.45917	0.14653	0.00037	0.01854	0.00003	6.20432	0.01039	94.39	0.28

078-12 PB-108 BI 07-28-99 PEBBLE

Weighted average of J from standards = 0.008658 +/- 0.000022

Laser Power (mW)	Cumulative 39Ar	40Ar/39Ar measured	+/-	37Ar/39Ar measured	+/-	36Ar/39Ar measured	+/-	% Atmospheric 40Ar	Ca/K	+/-	Cl/K	+/-	40*/39K	+/-	Age (Ma)	+/- (Ma)
150	0.0003	356.4129	11.12089	3.12067	0.16329	1.18176	0.04176	97.92107	5.73765	0.30084	1.16171	0.03704	7.42406	5.90943	112.38	86.73
300	0.0016	170.7389	1.38411	1.88968	0.04213	0.50589	0.00901	87.48672	3.47158	0.07748	1.04993	0.01009	21.38776	2.40456	306.49	31.69
600	0.0102	36.53939	0.08824	0.76414	0.01015	0.0958	0.00065	77.38275	1.40279	0.01864	0.30715	0.00108	8.26183	0.1831	124.64	2.67
750	0.02	13.59506	0.09455	1.3039	0.01243	0.02596	0.0005	55.81865	2.3945	0.02284	0.11855	0.00122	5.9989	0.14553	91.35	2.16
900	0.0344	9.77007	0.04854	1.95115	0.01066	0.01352	0.00035	39.50787	3.58465	0.01961	0.10781	0.00067	5.90028	0.10769	89.88	1.6
1050	0.0575	8.58919	0.03357	2.97158	0.01411	0.00939	0.00021	29.80523	5.46301	0.02598	0.09988	0.00057	6.0207	0.06564	91.67	0.97
1250	0.1088	7.2209	0.01181	3.56743	0.00759	0.00429	0.00013	13.90107	6.56098	0.01399	0.08232	0.00026	6.20688	0.04106	94.43	0.61
1500	0.1947	6.98583	0.01209	3.63317	0.00637	0.00359	0.00007	11.32542	6.68217	0.01174	0.08529	0.00023	6.18389	0.02364	94.09	0.35
1750	0.2856	6.9657	0.01097	3.92505	0.0083	0.00343	0.00009	10.34727	7.22038	0.0153	0.09112	0.00023	6.23521	0.02805	94.85	0.42
2000	0.4	6.85129	0.00614	3.77237	0.00384	0.00293	0.00008	8.55346	6.93882	0.00707	0.09427	0.00029	6.25445	0.02573	95.14	0.38
2250	0.5367	6.74792	0.0076	3.69839	0.00535	0.00244	0.00007	6.58036	6.80241	0.00986	0.07719	0.00014	6.29229	0.02257	95.7	0.33
2500	0.6361	6.6804	0.00586	3.76938	0.00677	0.00231	0.00011	5.99517	6.9333	0.01248	0.08042	0.00017	6.26836	0.03231	95.34	0.48
2750	0.7404	6.71723	0.01193	3.87707	0.00866	0.00243	0.00006	6.36858	7.1319	0.01597	0.09409	0.00027	6.27848	0.02015	95.49	0.3
3000	0.8294	6.50367	0.01194	3.52267	0.0081	0.00165	0.00007	3.42555	6.47847	0.01493	0.07056	0.00021	6.2676	0.02424	95.33	0.36
3500	0.9387	6.60841	0.00599	3.53315	0.00508	0.00212	0.00006	5.46821	6.4978	0.00936	0.06898	0.00009	6.23432	0.01742	94.84	0.26
8500	1	6.50897	0.01352	3.35064	0.0089	0.00266	0.0001	8.24251	6.1614	0.0164	0.05872	0.00016	5.95919	0.03181	90.76	0.47
Integrated		7.48418	0.00331	3.59278	0.00208	0.00501	0.00003	16.2543	6.60771	0.00383	0.08576	0.00007	6.25834	0.00905		

UAF082-656 BJT-68 BI 10-19-00 PEBBLE COPPER

Weighted average of J from standards = 0.008971 +/- 0.000024

Laser Power (mW)	Cumulative 39Ar	40Ar/39Ar measured	+/-	37Ar/39Ar measured	+/-	36Ar/39Ar measured	+/-	% Atmospheric 40Ar	Ca/K	+/-	Cl/K	+/-	40*/39K	+/-	Age (Ma)	+/- (Ma)
150	0.0023	56.63511	0.2892	0.2485	0.00203	0.17565	0.00096	91.65883	0.45604	0.00373	0.01926	0.00022	4.7224	0.28723	74.85	4.46
200	0.0047	24.16113	0.12457	0.52881	0.0028	0.06391	0.00066	78.09386	0.97064	0.00513	0.00799	0.00019	5.28831	0.19991	83.62	3.09
300	0.0202	9.98604	0.08937	0.08115	0.0007	0.01383	0.00016	40.98979	0.14891	0.00128	0.0092	0.00009	5.87616	0.08295	92.68	1.28
450	0.0756	6.94104	0.0197	0.00751	0.00007	0.00356	0.00003	15.20401	0.01378	0.00012	0.00904	0.00004	5.86141	0.02027	92.45	0.31
600	0.1409	6.23343	0.01463	0.00301	0.00004	0.00159	0.00002	7.54618	0.00553	0.00007	0.00765	0.00004	5.73652	0.0147	90.53	0.23
750	0.204	6.03992	0.01249	0.00257	0.00004	0.00115	0.00001	5.64569	0.00472	0.00008	0.00612	0.00003	5.67185	0.01294	89.54	0.2
900	0.2658	5.94949	0.01408	0.00304	0.00005	0.00092	0.00001	4.59178	0.00557	0.00009	0.00564	0.00003	5.64893	0.01426	89.18	0.22
1100	0.3418	5.87144	0.01448	0.00315	0.00003	0.00076	0.00001	3.83813	0.00579	0.00006	0.00629	0.00003	5.6185	0.01461	88.71	0.23
1400	0.451	5.80321	0.01345	0.00276	0.00003	0.00058	0.00001	2.96963	0.00506	0.00006	0.00764	0.00004	5.60304	0.0136	88.47	0.21
1700	0.5622	5.78199	0.01685	0.00353	0.00003	0.0005	0.00001	2.58858	0.00648	0.00006	0.00864	0.00003	5.60437	0.01678	88.5	0.26
2000	0.6623	5.77002	0.01778	0.00377	0.00004	0.00049	0.00001	2.5279	0.00692	0.00007	0.00882	0.00004	5.5962	0.01774	88.37	0.27
2500	0.763	5.78352	0.01602	0.00617	0.00004	0.00054	0.00001	2.75552	0.01133	0.00008	0.00883	0.00003	5.59627	0.01609	88.37	0.25
3000	0.8505	5.8024	0.01805	0.00684	0.00004	0.00061	0.00001	3.13697	0.01254	0.00008	0.00867	0.00004	5.59261	0.01805	88.31	0.28
3500	0.9072	5.7955	0.018	0.02189	0.00021	0.00061	0.00001	3.10062	0.04016	0.00038	0.00848	0.00003	5.58807	0.0183	88.24	0.28
8000	1	5.82818	0.01957	0.07507	0.00024	0.00076	0.00001	3.79898	0.13775	0.00045	0.00828	0.00004	5.57943	0.01943	88.11	0.3
Integrated		6.14347	0.00504	0.01481	0.00003	0.00164	0	7.91724	0.02717	0.00005	0.00799	0.00001	5.63071	0.00505	88.9	0.25

078-13 PB-162 WR 07-28-99 PEBBLE

Weighted average of J from standards = 0.008658 +/- 0.000022

Laser Power (mW)	Cumulative 39Ar	40Ar/39Ar measured	+/-	37Ar/39Ar measured	+/-	36Ar/39Ar measured	+/-	% Atmospheric 40Ar	Ca/K	+/-	Cl/K	+/-	40*/39K	+/-	Age (Ma)	+/- (Ma)
150	0.0031	40.66716	0.17082	0.03087	0.00235	0.11515	0.00172	83.72188	0.05665	0.00431	0.0105	0.00019	6.61531	0.49006	100.48	7.24
300	0.0171	11.6901	0.03475	0.02449	0.00075	0.02027	0.00031	51.34021	0.04494	0.00138	0.00186	0.00013	5.6745	0.09334	86.52	1.39
600	0.1102	6.48355	0.03151	0.01433	0.0001	0.00269	0.00005	12.29759	0.02629	0.00019	0.0008	0.00003	5.66111	0.03432	86.32	0.51
750	0.1903	5.85104	0.03756	0.00864	0.00013	0.00063	0.00003	3.20907	0.01585	0.00025	0.00064	0.00001	5.63553	0.03838	85.94	0.57
900	0.2683	5.77389	0.03245	0.00664	0.00017	0.00042	0.00002	2.13578	0.01219	0.00031	0.00066	0.00004	5.62251	0.03296	85.75	0.49
1050	0.3508	5.77698	0.01154	0.00588	0.00011	0.00033	0.00002	1.6915	0.01079	0.00021	0.00056	0.00002	5.65107	0.01319	86.17	0.2
1250	0.4474	5.78618	0.0179	0.00605	0.0001	0.0005	0.00003	2.5474	0.0111	0.00019	0.00057	0.00001	5.61084	0.02006	85.58	0.3
1500	0.5501	5.82426	0.01234	0.00771	0.00013	0.00076	0.00002	3.88032	0.01416	0.00023	0.00062	0.00002	5.57071	0.01405	84.98	0.21
1750	0.6325	5.98522	0.02486	0.00989	0.00022	0.00115	0.00003	5.70957	0.01815	0.00041	0.00066	0.00002	5.61646	0.02668	85.66	0.4
2000	0.6951	5.99159	0.00693	0.00873	0.0002	0.00102	0.00004	5.0497	0.01602	0.00037	0.0006	0.00002	5.66181	0.01485	86.33	0.22
2250	0.7448	6.00245	0.01287	0.00899	0.00027	0.00099	0.00006	4.86787	0.01649	0.0005	0.00066	0.00005	5.68299	0.02059	86.65	0.31
2500	0.7884	6.04889	0.00824	0.00971	0.00037	0.00117	0.00007	5.75505	0.01782	0.00068	0.00068	0.00003	5.67376	0.0212	86.51	0.32
2750	0.8287	6.09481	0.00647	0.01101	0.00037	0.00127	0.00006	6.18306	0.0202	0.00068	0.00073	0.00004	5.69108	0.01996	86.77	0.3
3000	0.8544	6.13033	0.01354	0.01215	0.00037	0.00141	0.00008	6.79544	0.02229	0.00068	0.00067	0.00002	5.68704	0.02638	86.71	0.39
3500	0.8878	6.20755	0.00691	0.01257	0.00028	0.00165	0.00006	7.87329	0.02307	0.00052	0.00078	0.00005	5.69242	0.01848	86.79	0.28
8500	1.0001	6.36102	0.02265	0.03919	0.00014	0.00235	0.00002	10.9263	0.07191	0.00025	0.00088	0.00001	5.64058	0.02315	86.02	0.34
8500	1	-13.6886	0.65616	-0.02116	0.14242	-0.03165	0.024	68.16552	-0.03882	0.26132	0.00172	0.00577	-4.36678	7.08384	-69.53	114.99
Integrated		6.20297	0.00643	0.01266	0.00005	0.0018	0.00001	8.5913	0.02322	0.0001	0.00072	0.00001	5.64387	0.00733	86.07	0.24

078-11 PB-79 BI 07-27-99 PEBBLE

Weighted average of J from standards = 0.008658 +/- 0.000022

Laser Power (mW)	Cumulative 39Ar	40Ar/39Ar measured	+/-	37Ar/39Ar measured	+/-	36Ar/39Ar measured	+/-	% Atmospheric 40Ar	Ca/K	+/-	Cl/K	+/-	40*/39K	+/-	Age (Ma)	+/- (Ma)
150	0.0051	204.8094	1.78362	0.07993	0.00995	0.66536	0.00795	96.009	0.14666	0.01825	0.09987	0.00136	8.17322	1.61701	123.35	23.59
300	0.0275	19.85519	0.06331	0.07087	0.00322	0.05071	0.0008	75.5531	0.13003	0.00591	0.03038	0.00035	4.84719	0.23379	74.16	3.5
600	0.1473	9.03904	0.01444	0.03862	0.00072	0.01165	0.00012	38.17794	0.07086	0.00133	0.03434	0.00013	5.57052	0.03736	84.97	0.56
750	0.2469	7.02339	0.01404	0.11247	0.0009	0.00507	0.00012	21.29837	0.20639	0.00165	0.03296	0.00019	5.50534	0.03763	84	0.56
900	0.3398	6.71099	0.00931	0.05366	0.00083	0.00375	0.00006	16.52396	0.09846	0.00152	0.03176	0.00022	5.57831	0.01968	85.09	0.29
1050	0.4297	6.46473	0.02332	0.07661	0.00092	0.00325	0.00009	14.84403	0.14057	0.0017	0.03125	0.00021	5.48094	0.03463	83.64	0.52
1250	0.5207	6.29879	0.01349	0.10922	0.00086	0.0029	0.00009	13.52333	0.20042	0.00159	0.03174	0.00023	5.42255	0.02909	82.77	0.43
1500	0.6198	6.27276	0.01676	0.14189	0.00172	0.00285	0.0001	13.30676	0.26037	0.00315	0.03124	0.00013	5.41368	0.03358	82.64	0.5
1750	0.7137	6.38163	0.01229	0.15405	0.00154	0.00262	0.0001	11.99977	0.28268	0.00282	0.03387	0.00018	5.59116	0.03032	85.28	0.45
2000	0.7681	6.27329	0.02468	0.10858	0.00192	0.00264	0.00024	12.35464	0.19924	0.00352	0.03435	0.00037	5.47348	0.07368	83.53	1.1
2250	0.7998	6.17009	0.02093	0.11608	0.00203	0.00262	0.00053	12.48152	0.21301	0.00372	0.03451	0.00039	5.37526	0.15919	82.06	2.38
2500	0.8315	6.26248	0.02489	0.11697	0.00386	0.00281	0.00038	13.18181	0.21464	0.00708	0.03437	0.00022	5.41247	0.11363	82.62	1.7
2750	0.8586	6.44528	0.04102	0.08396	0.00326	0.0026	0.00044	11.8818	0.15406	0.00598	0.03438	0.00036	5.65449	0.13409	86.23	2
3000	0.9152	5.9831	0.01523	0.11033	0.00218	0.00187	0.00021	9.15226	0.20245	0.00401	0.03278	0.00019	5.40983	0.06389	82.58	0.95
3500	0.9512	6.52892	0.03249	0.14242	0.00289	0.00309	0.0004	13.89777	0.26135	0.00529	0.03379	0.00056	5.59735	0.12244	85.37	1.82
8500	1	6.5497	0.02935	0.17003	0.00237	0.0029	0.00024	12.93277	0.31202	0.00435	0.03633	0.00027	5.67828	0.07406	86.58	1.1
Integrated		8.08289	0.00577	0.10341	0.00041	0.00864	0.00006	31.59637	0.18975	0.00075	0.03334	0.00006	5.50973	0.01683	84.07	0.33

078-08 S-91 KS 07-28-99 PEBBLE

Weighted average of J from standards = 0.008658 +/- 0.000022

Laser Power (mW)	Cumulative 39Ar	40Ar/39Ar measured	+/-	37Ar/39Ar measured	+/-	36Ar/39Ar measured	+/-	% Atmospheric 40Ar	Ca/K	+/-	Cl/K	+/-	40*/39K	+/-	Age (Ma)	+/- (Ma)
150	0.0053	46.41887	0.28836	0.03828	0.00198	0.14372	0.00126	91.54459	0.07025	0.00363	0.00346	0.00034	3.92257	0.26746	60.25	4.04
300	0.0566	8.42609	0.00901	0.01574	0.00026	0.01788	0.00016	62.88911	0.02889	0.00047	0.0006	0.00005	3.11638	0.04864	48.03	0.74
600	0.1588	5.03779	0.00784	0.01284	0.00035	0.00675	0.00004	39.80627	0.02355	0.00064	0.00043	0.00001	3.01518	0.0132	46.49	0.2
750	0.2145	4.22489	0.00651	0.01067	0.00045	0.00385	0.00008	27.10337	0.01958	0.00082	0.00041	0.00005	3.0589	0.02525	47.16	0.38
900	0.2721	3.8068	0.00708	0.01179	0.00045	0.00261	0.00007	20.40239	0.02163	0.00083	0.00046	0.00002	3.0073	0.02194	46.37	0.33
1050	0.33	3.62664	0.00329	0.01156	0.00034	0.00198	0.00006	16.20163	0.0212	0.00063	0.00048	0.00002	3.01504	0.01654	46.49	0.25
1250	0.3994	3.52049	0.00451	0.01162	0.00025	0.00174	0.00003	14.69842	0.02133	0.00046	0.00049	0.00004	2.97858	0.01057	45.93	0.16
1500	0.4915	3.58714	0.00645	0.01468	0.00036	0.00191	0.00004	15.84905	0.02693	0.00066	0.00052	0.00004	2.99449	0.01394	46.18	0.21
1750	0.5714	3.7367	0.00322	0.01867	0.00041	0.00234	0.00004	18.62417	0.03426	0.00075	0.0006	0.00004	3.01746	0.01121	46.53	0.17
2000	0.6346	3.85519	0.00682	0.01924	0.00044	0.00269	0.00007	20.7007	0.03531	0.00082	0.00055	0.00003	3.03442	0.02188	46.78	0.33
2250	0.6983	4.09618	0.00582	0.02548	0.00023	0.0035	0.00006	25.37179	0.04675	0.00043	0.0006	0.00004	3.03554	0.01978	46.8	0.3
2500	0.7494	4.0024	0.00736	0.02502	0.00063	0.00322	0.0001	23.90566	0.0459	0.00116	0.0007	0.00005	3.02381	0.02929	46.62	0.45
2750	0.8022	4.0619	0.01244	0.0298	0.00038	0.00348	0.00006	25.4528	0.05469	0.0007	0.00072	0.00004	3.0067	0.02075	46.36	0.32
3000	0.8526	4.23607	0.00777	0.03878	0.00047	0.00402	0.0001	28.14101	0.07116	0.00087	0.00083	0.00005	3.02345	0.02989	46.62	0.45
3500	0.9093	4.69158	0.00606	0.02987	0.00035	0.00547	0.00009	34.61234	0.0548	0.00065	0.00091	0.00003	3.049	0.02669	47.01	0.41
8500	1	5.31893	0.01124	0.04759	0.00059	0.00754	0.00007	42.04446	0.08733	0.00108	0.00107	0.00003	3.06608	0.02242	47.27	0.34
Integrated		4.61637	0.00204	0.02157	0.00011	0.00527	0.00002	33.90327	0.03958	0.0002	0.00064	0.00001	3.03234	0.00576	46.75	0

APPENDIX C

SUMMARY DRILL HOLE LOGS OF SELECTED HOLES.

See key for abbreviations

DDH	PB24		Collar Elev.	1516.1
Northing	50531		Bearing	360
Easting	54981		Angle	90
			depth	209.0
Elev. (start)	Elev. (end)	lith	altn. (most to least)	notes
1516.1	1508.1	OB	FeO	
1508.1	1307.1	Kd	py	geochron sample PB-108, 144' depth
	EOH			

DDH	PB28		Collar Elev.	1089.0
Northing	56134		Bearing	360
Easting	61316		Angle	90
			depth	297.0
Elev. (start)	Elev. (end)	lith	altn. (most to least)	notes
1089.0	1029	OB	FeO	
1029.0	960.5	Kgde	ser, kfs, bt	
960.5	907	Kibx	ser, kfs, bt	
907.0	902.5	Ta dike	ser, kfs, bt	
902.5	792	Kibx	bt, kfs, ser	geochron.sample BJT-68, 203' depth
	EOH			

Key: All lithology codes are shown in Figure 1 of the text, except the following additions: Tlp = Tertiary porphyritic latite, Tle = Tertiary equigranular latite, and OB = overburden. Alteration/mineralization abbreviations are: FeO = iron oxide, ser = sericite, sil = silicification, kfs = K-feldspar, bt = biotite, chl = chlorite, cc = calcite, py = pyrite, qtz = quartz, and carb = carbonate

See key for abbreviations

DDH	PB78		Collar Elev.	1172.6
Northing	57408		Bearing	360
Easting	60577		Angle	90
			depth	600.0
Elev. (start)	Elev. (end)	lith	altn. (most to least)	notes
1172.6	1132.6	OB		
1132.6	1096.4	Kh	kfs, bt	
1096.4	1093.1	Kgdp	kfs, bt	
1093.1	1066.6	Kh	kfs, bt	
1066.6	1032.6	Kgdp	kfs, bt	
1032.6	986.1	Kgdb	kfs, bt	
986.1	974.6	Kbd	kfs, bt	geochron sample PB-162, 193' depth
974.6	945.6	Kgdp	kfs, bt	
945.6	917.6	Kbd	kfs, bt	
917.6	910.4	Kgdp	kfs, bt	
910.4	904.9	Kgdb	bt, kfs	
904.9	890.1	Kgdp	kfs, bt	
890.1	882.5	Kgdb	kfs, bt	
882.5	876.1	Kgdp	kfs, bt	
876.1	852.6	Kgdb	kfs, bt	
852.6	795.6	Kh	kfs, bt	
795.6	788	Kgdb	kfs, bt	
788.0	754.4	Kh	kfs, bt	
754.4	748.6	Kgdb	kfs, bt	
748.6	744.3	Kh	kfs, bt	
744.3	737.6	Kgdb	kfs, bt	
737.6	730.6	Kh	kfs, bt	

continued

DDH	PB78		Collar Elev.	1172.6
Northing	57408		Bearing	360
Easting	60577		Angle	90
			depth	600.0
Elev. (start)	Elev. (end)	lith	altn. (most to least)	notes
730.6	723.3	Kgdb	kfs, bt	
723.3	572.6	Kgdp	kfs, bt	
	EOH			

See key for abbreviations

DDH	PB39		Collar Elev.	1284.1
Northing	58351		Bearing	320
Easting	61593		Angle	45
			depth	515.0
Elev. (start)	Elev. (end)	lith	altn. (most to least)	notes
1284.1	1281.0	OB		
1281.0	1185.9	Kgde	bt, ser	
1185.9	1063.4	Kgdp	bt, kfs, ser	
1063.4	1060.3	Ta dike	bt, kfs, ser, cc	geochron sample PB-83, 169' depth (N:58442, E: 61502)
1060.3	1012.4	Kgdp	bt, kfs, ser	
1012.4	904.0	Kh	bt, kfs, ser	
904.0	879.6	Kd/Kgb	bt, kfs, ser, chl	
	EOH			

See key for abbreviations

DDH	PB105		Collar Elev.	1225.0
Northing	41800		Bearing	360
Easting	60800		Angle	90
			depth	323.0
Elev. (start)	Elev. (end)	lith	altn. (most to least)	notes
1225.0	1224.0	OB		
1224.0	902.0	Ksy	py (minor)	geochron sample PB-79, 74' depth
	EOH			

See key for abbreviations

DDH	S19		Collar Elev.	1172.6
Northing	?		Bearing	360
Easting	?		Angle	-50
			depth	536.0
Elev. (start)	Elev. (end)	lith	altn. (most to least)	notes
1172.6	1139.8	Tle		weathered
1139.8	1109.8	Tlp	ser, sil, clay	altered shear zone
1109.8	1072.1	Tlp	variable sil	
1072.1	1057.4	Tlp	variable sil	sil.veining and brecciated, Au to .17 opt
1057.4	946.4	Tlp/Tle	variable sil	qtz veined
946.4	841.7	Tlp	kfs, sil	veined, geochron sample S-91 at 449' depth
841.7	830.2	Tlp	kfs, sil	
830.2	801.0	Tlp	kfs, sil	heavy veining: qtz-pseudo carb, brecciated
801.0	798.4	Tlp	sil	
		EOH		